Cellular/Molecular

Localization of the Endocannabinoid-Degrading Enzyme Fatty Acid Amide Hydrolase in Rat Dorsal Root Ganglion Cells and Its Regulation after Peripheral Nerve Injury

Isobel J. Lever,[1] Michelle Robinson,[3] Mario Cibelli,[2] Cleoper Paule,[1] Peter Santha,[1] Louis Yee,[1] Stephen P. Hunt,[3] Benjamin F. Cravatt,[4] Maurice R. Elphick,[5] Istvan Nagy,[1] and Andrew S. C. Rice[1]

[1]Pain Research Group and [2]Department of Anaesthetics, Pain Medicine and Intensive Care, Faculty of Medicine, Imperial College London, Chelsea and Westminster Hospital Campus, London SW10 9NH, United Kingdom, [3]Department of Anatomy and Developmental Biology, University College London, London WC1E 6BT, United Kingdom, [4]The Skaggs Institute for Chemical Biology and Departments of Cell Biology and Chemistry, The Scripps Research Institute, La Jolla, California 92037, and [5]School of Biological and Chemical Sciences, Queen Mary, University of London, London E1 4NS, United Kingdom

Fatty acid amide hydrolase (FAAH) is a degradative enzyme for a group of endogenous signaling lipids that includes anandamide (AEA). AEA acts as an endocannabinoid and an endovanilloid by activating cannabinoid and vanilloid type 1 transient receptor potential (TRPV1) receptors, respectively, on dorsal root ganglion (DRG) sensory neurons. Inhibition of FAAH activity increases AEA concentrations in nervous tissue and reduces sensory hypersensitivity in animal pain models. Using immunohistochemistry, Western blotting, and reverse transcription-PCR, we demonstrate the location of the FAAH in adult rat DRG, sciatic nerve, and spinal cord. In naive rats, FAAH immunoreactivity localized to the soma of 32.7 ± 0.8% of neurons in L4 and L5 DRG. These were small-sized (mean soma area, 395.96 ± 5.6 μm^2) and predominantly colabeled with peripherin and isolectin B4 markers of unmyelinated C-fiber neurons; 68% colabeled with antibodies to TRPV1 (marker of nociceptive DRG neurons), and <2% colabeled with NF200 (marker of large myelinated neurons). FAAH-IR was also present in small, NF200-negative cultured rat DRG neurons. Incubation of these cultures with the FAAH inhibitor URB597 increased AEA-evoked cobalt uptake in a capsazepine-sensitive manner. After sciatic nerve axotomy, there was a rightward shift in the cell-size distribution of FAAH-immunoreactive (IR) DRG neurons ipsilateral to injury: FAAH immunoreactivity was detected in larger-sized cells that colabeled with NF200. An ipsilateral versus contralateral increase in both the size and proportion of FAAH-IR DRG occurred after spinal nerve transection injury but not after chronic inflammation of the rat hindpaw 2 d after injection of complete Freund's adjuvant. This study reveals the location of FAAH in neural tissue involved in peripheral nociceptive transmission.

Introduction

The endogenous ligands for cannabinoid receptors (endocannabinoids) are rapidly synthesized inside activated neurons (Di Marzo et al., 1994; Piomelli et al., 1998). Tissue concentrations of endocannabinoids increase locally after injury (Calignano et al., 1998; Baker et al., 2001; Dinis et al., 2004) or ischemia (Muthian et al., 2004) and are elevated in paw skin and in the periaqueductal gray (PAG) brain region after Formalin injury, providing evidence of activity-dependent endocannabinoid production in nociceptive pathways (Calignano et al., 1998; Walker et al., 1999).

When injected into rat skin after inflammation or nerve injury, the endocannabinoid anandamide (AEA) mediates analgesic effects via the activation of peripheral cannabinoid receptors (CBRs) (Calignano et al., 1998; Richardson et al., 1998; Guindon and Beaulieu, 2006). AEA signaling at CBRs is relatively transient because of the short half-life of AEA in tissue (Di Marzo et al., 1994). AEA is inactivated by cellular reuptake, followed by hydrolysis or oxidative degradation (Deutsch and Chin 1993; Kozak and Marnett, 2002). Hydrolysis is catalyzed by a membrane-bound serine hydrolase enzyme, fatty acid amide hydrolase (FAAH) (Cravatt et al., 1996; Deutsch et al., 2002).

FAAH activity regulates AEA levels in tissue because inhibition of the enzyme or disruption of the *faah* gene in knock-out mice ($FAAH^{-/-}$), both cause substantial increases in AEA concentrations measured in rodent brain and spinal cord (Cravatt et al., 2001; Lichtman et al., 2004a; Hohmann et al., 2005). FAAH inactivation can reduce pain-related behavior by increasing AEA signaling at CBRs (Cravatt et al., 2001, 2004), reducing hyperreflexic responses after inflammatory (Lichtman et al., 2004b; Holt et al., 2005; Jayamanne et al., 2006) or neuropathic injury (Chang et al., 2006; Jhaveri et al., 2006; Russo et al., 2007), and enhancing stress-induced analgesia (Hohmann et al., 2005).

Extracellular AEA can activate CBRs *in vitro*, inhibiting the activity of small, C-fiber dorsal root ganglion (DRG) neurons of the type that transmit nociceptive input to the CNS (Richardson et al., 1998; Ross et al., 2001; Ahluwalia et al., 2003a). These neurons express vanilloid type 1 transient receptor potential

Received Aug. 26, 2008; revised Nov. 4, 2008; accepted Jan. 14, 2009.

This work was supported by the Wellcome Trust (London Pain Consortium).

Correspondence should be addressed to Prof. Andrew S. C. Rice, Pain Research Group, Department of Anaesthetics, Pain Medicine and Intensive Care, Imperial College London, Chelsea and Westminster Hospital Campus, 369 Fulham Road, London SW10 9NH, UK. E-mail: a.rice@imperial.ac.uk.

DOI:10.1523/JNEUROSCI.4071-08.2009

 0270-6474/09/293766-15$15.00/0

(TRPV1) receptors that are activated by capsaicin and noxious heat and are critical to the development of inflammatory thermal hyperalgesia (Caterina et al., 1997, 2000). AEA production has been measured in capsaicin-sensitive DRG neurons and can excite DRG neurons intracellularly by activation of TRPV1 receptors (Ahluwalia et al., 2003a; van der Stelt et al., 2005).

Neurons that produce AEA are also likely to contain FAAH (van der Stelt et al., 2005; Millns et al., 2006). In rodent CNS, this status is supported by the proximity of FAAH-immunoreactive (IR) neurons to AEA-responsive CBRs (Egertová et al., 1998, 2003; Gulyas et al., 2004). FAAH expression is reported in areas concerned with nociceptive transmission (PAG, thalamus, and the spinal cord) (Tsou et al., 1998). However, nothing is known about the cellular distribution of FAAH in primary sensory neurons. This study examines the expression of FAAH immunoreactivity in the DRG and spinal cord and investigates changes associated with nerve injury and inflammatory states.

Materials and Methods

Adult male Wistar rats of 250–300 g were used for all experiments, which were conducted according to United Kingdom Home Office regulations.

Sciatic nerve surgery. Rats were anesthetized by inhalation of 1–2% isoflurane (Abbott Laboratories) in O_2 and N_2O, and one of the following aseptic procedures was applied to the left sciatic nerve. For axotomy, the nerve was exposed at midthigh level, tightly ligated with a 4.0 suture, and then sectioned. For spinal nerve transection (SNT), the L5 spinal nerve was exposed, tightly ligated, and sectioned 2–4 mm distal from the suture. Sham surgery was performed by exposing the appropriate part of the nerve in the absence of a ligation and sectioning injury. The time points at which the tissue was harvested after nerve injury ranged from 3 to 7 d after surgery. Sensory testing was conducted on SNT-injured animals to determine the establishment of hypersensitivity to mechanical and cold stimulation. Animals were placed in Plexiglas boxes with 0.8-cm-diameter mesh flooring and allowed to acclimatize for 15 min or until exploratory behavior ceased. For testing mechanical hypersensitivity, an electronic von Frey device (Moller et al., 1998), with a probe tip area of 0.5 mm^2 (Somedic Sales), was applied manually to the midplantar surface of the hindpaw at a rate of 8–15 g/s. The paw-withdrawal threshold was defined as the average force in grams that evoked an active limb-withdrawal response over five applications; at least 3 min elapsed between each test. Withdrawal to a cold stimulus was assessed using the acetone drop application technique modified from the work of Carlton et al. (1994). Sampling was performed by the application of a single bubble of acetone to the midplantar surface of each hindpaw from the tip of a 1 ml syringe. A positive response was recorded if the animal withdrew the paw after acetone application. The paw was sampled five times, and a mean was calculated. Mean ± SEM paw-withdrawal responses for mechanical and cooling stimuli, measured ipsilateral and contralateral to injury, were calculated for animals in each group on each testing day before and after surgery. Statistical comparisons were made between withdrawal responses (on different testing days or between different animal groups on the same testing day) using a one-way ANOVA, followed by the appropriate *post hoc* multiple comparison procedure. This was either a Tukey's or Dunn's test, or a Kruskal–Wallis one-way ANOVA on ranks using the Student–Newman–Keuls method.

Complete Freund's adjuvant-induced inflammation. Chronic inflammation of left rat hindpaws was induced by a 50 μl injection of 50% complete Freund's adjuvant (CFA) (Sigma-Aldrich). As described previously, the development of thermal hypersensitivity was tested on the ipsilateral and contralateral side to CFA inflammation, 2 d after injection using the plantar test (Hargreaves et al., 1988). Animals were placed in Plexiglas boxes, and, after the acclimatization period, timed paw-withdrawal response latencies were measured in response to an infrared beam (thermal stimulus) (Ugo Basile) positioned under the plantar surface of the paw. The mean ± SEM of three withdrawal responses was calculated per paw, and the data were analyzed as described for responses to mechanical and cold stimulation.

Immunohistochemistry. Rats were anesthetized with sodium pentobarbital (60 mg/kg) and perfused through the ascending aorta with 100 ml of 0.9% saline and then 300 ml of 4% paraformaldehyde in 0.1 M phosphate buffer (PB), pH 7.4. Lumbar (L4 and L5) DRG were located by tracing the lumbar dorsal roots back to the sciatic nerve. Dissected tissue was post-fixed for 1–2 h at 4°C, cryoprotected in 15–30% sucrose in 0.1 M PB for 12 h at 4°C, and embedded in mounting medium. Cryosections were cut and thaw mounted onto Superfrost slides (VWR) at the following thicknesses: coronal brain, 30 μm; transverse spinal cord, 20 μm; sciatic nerve, 10 μm; and DRG, 10 μm. Fresh-frozen tissue from $FAAH^{-/-}$ or $FAAH^{+/+}$ mice (Ledent et al., 1999) (obtained from a colony maintained by Prof. David Baker, Institute of Neurology, UCL, London, UK) were cryosectioned and fixed in acetone. For paraffin sections, postfixed tissue was embedded in paraffin wax and cut at 5 μm thickness on a vibraslice. Dried and dewaxed sections were processed identically for immunohistochemistry. Slides were incubated with PBST (0.1 M phosphate buffer, 0.1% sodium azide, 0.3% Triton X-100, and 0.3 M NaCl) containing 10% normal donkey serum for 1 h at room temperature. A rabbit primary antibody raised to a truncated form of rat FAAH protein, ΔTM FAAH comprising amino acids 38–579 as described previously (Patricelli et al., 1998; Cravatt et al., 2001) was diluted 1:2000 in PBST containing one of the following costaining primary antibodies: mouse anti neuronal-specific nuclear protein (NeuN) at 1:2000 (Millipore Bioscience Research Reagents), sheep anti-calcitonin gene-related peptide (CGRP) at 1:2000 (Affinity BioReagents), mouse anti-NF200 (N52) at 1:1 to 1:2000 (Sigma-Aldrich), or goat anti-peripherin at 1:100 (Santa Cruz Biotechnology). Slides were incubated with antibody mixtures for 48 h at room temperature and processed for signal amplification using avidin–biotin (Vector Laboratories) and tyramide reagents [tyramide signal amplification (TSA)] (PerkinElmer Life and Analytical Sciences). This was followed by a 2 h incubation with fluorescent 5-(4,6-dichlorotriazinyl)-aminofluorescein or rhodamine-conjugated streptavidin antibodies (1:200; The Jackson Laboratory) together with an appropriate fluorophore-conjugated secondary antibody raised against the costaining primary antibody. Fluorescein-labeled *Griffonia simplicifolia* isolectin B4 (IB4) (Sigma-Aldrich) was incubated at 10 μg/ml for 1 h during the final incubation step for FAAH staining. Slides were mounted in Vectashield medium containing a 4′,6′-diamidino-2-phenylindole (DAPI) nuclear counterstain (Vector Laboratories). Costaining of FAAH with other rabbit antibodies [anti-TRPV1 at 1:1000 (Affinity BioReagents), anti-S100 at 1:1200 (Dako), and anti-activating transcription factor 3 (ATF3) (Santa Cruz Biotechnology)] was performed subsequent to the TSA procedure for the FAAH antibody, as described previously (Michael et al., 1997). Costaining of spinal cord tissue with type 1 cannabinoid receptor (CB_1) antibodies was performed with TSA, followed by incubation of FAAH antibodies at 1:200. The rabbit CB_1 antibody used was raised to amino acids 461–473 of the C-terminal domain of the rat CB_1 receptor [affinity purified from antiserum 2824.4(2) (Egertová and Elphick, 2000)] and incubated at 1:10 for 64 h at room temperature. Controls for FAAH immunohistochemistry included the following: (1) omission of the primary antibody, (2) preabsorption of the FAAH antibody at 1:1000 with the immunizing peptide at 10 μg/ml for 1 h at room temperature followed by tissue incubation with the preabsorbed antibody, (3) testing the antibody on tissue from $FAAH^{-/-}$ mice (Ledent et al., 1999), and (4) use of an alternative rabbit polyclonal antibody raised against a 17 aa immunogen from the N terminus of human FAAH protein (immunogen 100% conserved in rat) (Millipore Bioscience Research Reagents).

Image analysis and quantification of immunofluorescent DRG cells. Immunofluorescent images were visualized using a Leica DMR Fluorescence microscope and captured on a Hamamatsu CCD camera using QWIN image processing software (Leica). Quantification of the images from immunopositive DRG cells was semiautomated using software-based measurement of fluorescence intensity. The standard threshold grayscale intensity for detection of FAAH-immunoreactive cells was set at 130–255 arbitrary units (a.u.) and applied uniformly to all DRG images captured under identical illumination and exposure conditions. At least 100 DRG cells were randomly sampled per animal from serial sections at a distance of >10 sections apart from each other. Outlines of

DRG cell profiles containing a DAPI- or NeuN-labeled nucleus were drawn over each image to produce an overlay of the nucleated cell profiles. Exclusion of non-nucleated, immunopositive cell profiles from the size analysis was designed to prevent inaccurate measurements of elliptical-shaped DRG neuronal soma measured in cross section (Potrebic et al., 2003). A version of the nucleated cell profile overlay was modified using threshold intensity measurements to represent the population of immunopositive nucleated profiles. Both overlays were used to count and make area and fluorescence intensity measurements of all nucleated DRG cell profiles, as well as immunopositive cells within this group. Analysis of DRG images from injured and uninjured rats was performed by an investigator who was blinded to the treatment groups. Measurements were expressed as mean ± SEM for DRG sections sampled from each animal and for animals in each experimental group. The percentage of NeuN-IR DRG neurons colabeled with another marker were calculated for each animal and expressed as a mean ± SEM per experimental group. Statistical comparisons were made between different experimental groups using Student's *t* tests or one-way ANOVAs, together with the appropriate *post hoc* multiple comparison procedure.

Western blotting. Frozen tissue samples were thawed to 4°C and homogenized in lysis buffer: 50 mM Tris, pH 8.0, 100 mM NaCl, 10% glycerol, 1% Triton X-100, 5 mM EDTA, 1 mM PMSF, 10 μg/ml antipain, 10 μg/ml leupeptin, 1 mM sodium vanadate, 1 μg/ml pepstatin A (all from Sigma-Aldrich). Lysates were rotated for 1 h at 4°C and then centrifuged (10 min at 12,000 × *g*). Supernatants were collected and the total protein concentration determined using a BCA kit (Pierce via Perbio Science). Samples (normalized for protein concentration) were denatured in the appropriate PAGE loading buffer at 95°C for 5 min (or 70°C for 10 min for Bis-Tris gels). Protein extracts were separated using one of two electrophoresis systems: 10% Tris-HCl polyacrylamide gels (Bio-Rad) or NuPAGE Novex 4–12% Bis-Tris gels (Invitrogen) before transfer to nitrocellulose membranes. After blocking in a 6% solution of dried skimmed milk in TBST (Tris-HCl-buffered saline at pH 8.0 containing 0.05% Tween 20), blots were probed with ΔTM FAAH primary antibody (1:200 in block) at 4°C overnight. After detection using peroxidase-conjugated secondary antibody and chemiluminescence, membranes were stripped and reprobed with anti-glyceraldehyde-3-phosphate dehydrogenase (GAPDH) antibody (1:5000 in TBST at 4°C overnight; Abcam). Densitometric analysis of gel bands was performed using QWIN image analysis software (Leica). Briefly, images of the bands were captured under standard light conditions, and the optical densities of pixels sampled from images of each gel band were measured using a standard-sized area selection tool. Average pixel measurements derived from three separate gels were compared between different experimental groups using a one-way ANOVA and *post hoc* Tukey's test.

Reverse transcriptase-PCR. Reverse transcriptase (RT)-PCR was performed using samples from two L4 DRG per rat, ~30 mg of lumbar spinal cord or ~30 mg of hippocampal tissue. RNA was extracted according to the method of Akiba et al. (2004) using an RNeasy mini kit (Qiagen). Using a mastercycler (Eppendorf), reverse transcription proceeded at 42°C for 50 min, followed by a 15 min inactivation step at 70°C. A duplicate set of RNA samples (with the transcriptase enzyme omitted) was included in this reaction as a control for genomic DNA contamination in the PCR step. Both sample sets were run simultaneously for PCR amplification. PCR primers were designed across FAAH exon boundaries to prevent the amplification of genomic DNA (forward, 5′-GCC CTT CAG AGA GCA GCT CT-3′ designed across exons 7 and 8, intervening intron ~1159 bp; reverse, 5′-CTT TTC AGC TGA CCG AGG AC-3′ across exons 11 and 12, intervening intron ~265 bp). Database analysis with a basic local alignment search tool BLASTN search of GenBank was performed to assess and rule out potential hybridization with rat cDNA sequences other than FAAH. After 30 s denaturation at 96°C, the PCR reaction proceeded for 30 cycles of 1 min at 58°C for annealing and 3 min at 72°C for extension. PCR products were run on 2% agarose gels using standard protocols. The predicted size of the amplicon was 394 bp.

Dissociated DRG culture. DRG neurons were isolated from adult Sprague Dawley rats according to previously described methods (Singh Tahim et al., 2005). Briefly, coverslips bearing cultured cells were maintained at 37°C for >2 d. After three washes in PBS solution at 37°C, immunohistochemistry procedures were then performed at room temperature. Coverslips were fixed in 4% paraformaldehyde for 30 min, followed by PBS washes, incubation with PBST containing 10% normal donkey serum for 30 min, and then incubation with ΔTM FAAH primary antibody at 1:400 for 12 h. Costaining primary antibodies were either NeuN at 1:1000 or NF200 at 1:10,000. Secondary antibodies raised against rabbit and mouse IgG conjugated to cyanine 3 or FITC fluorophores (The Jackson Laboratory) were incubated for 1 h at 1:300 in PBST containing 4% normal donkey serum. Coverslips were slide mounted using Vectashield.

Table 1. Details of the preincubation and cobalt uptake buffers used in cobalt uptake experiments

Preincubation buffer solutions		Cobalt uptake buffer solutions	
Reagent	Concentration (μM)	Reagent	Concentration (μM)
URB597 (FAAH inhibitor)	1	Capsaicin	1
SR141716	1	AEA	1
URB597 +	1	URB597 +	1
SR1	1	AEA	1
URB597 +	1	URB597 +	1
Capsazepine	10	CAPZ	10
(TRPV1 antagonist)		SR141716	1
Buffer (control)		SR141716 +	1
		AEA	1
		SR141716 +	1
		URB597	1

A list of reagents and their concentrations when added to preincubation buffer solution or cobalt uptake buffer solution. Cultured DRG cells mounted on coverslips were transferred to one of the preincubation solutions for 5 min before transfer into a cobalt uptake buffer solution containing $CoCl_2$ for 5 min.

Cobalt uptake. TRPV1-mediated activation of cultured DRG neurons was assessed by cobalt uptake, as described previously (Sathianathan et al., 2003). Coverslips were washed for 2 min in buffer solution (in mM: 57.5 NaCl, 5 KCl, 2 $MgCl_2$, 10 HEPES, 12 glucose, and 139 sucrose, pH 7.4) and then preincubated for 5 min in buffer containing one of the following: the FAAH enzyme inhibitor URB597 (cyclohexylcarbamic acid 3-carbamoyl biphenyl-3-yl ester) (Mor et al., 2004; Fegley et al., 2005); buffer solution only (control); SR141716 [*N*-(piperidin-1-yl)-5-(4-chlorophenyl)-1-(2,4-dichlorophenyl)-4-methyl-3-pyrazole carboxamide] (CB_1 antagonist); URB597 + SR141716; or URB597 and the TRPV1 antagonist capsazepine (Table 1). Cells were then incubated in one of the buffer solutions containing 5 mM $CoCl_2$ (cobalt-uptake solution) as listed in Table 1.

Cobalt taken up by the neurons through activated nonselective cationic channels (Nagy et al., 1993) was precipitated by adding a 2.5% mercaptoethanol solution in buffer for 1 min. Cells were fixed in 70% ethanol. The cobalt precipitate (Co-ppt) was visualized by light microscopy. After background subtraction, images of labeled and nonlabeled cells were captured in grayscale, and their average optical intensity was measured within defined cell areas using QWIN image analysis software. Frequency distributions of optical intensity data (representing Co-ppt levels in >100 cells after each active or vehicle treatment) were fitted to Gaussian curves to determine the intensity threshold for Co-ppt-positive cells, as described previously (Sathianathan et al., 2003). Negative and positive control experiments were performed for each culture, in which control buffer or 10 μM capsaicin was added to the cobalt-containing buffer, respectively. Optical intensities from cells in the two types of experiment were fitted to Gaussian curves. The negative experiments represented two cell subpopulations, whereas three separate subpopulations were defined in the positive experiment. Mean optical intensity values for cells in the third subpopulation were higher than those of the two other subpopulations in both experiments and represented labeled cells. The cutoff point between the labeled and nonlabeled cells was determined as the mean value minus the 95% confidence interval for the third Gaussian curve in positive experiments. This optical intensity value was used to establish the relative number of labeled cells in all coverslips from the same culture. Data were presented as mean ± SEM. Differences in the relative number of labeled cells produced by various treatments

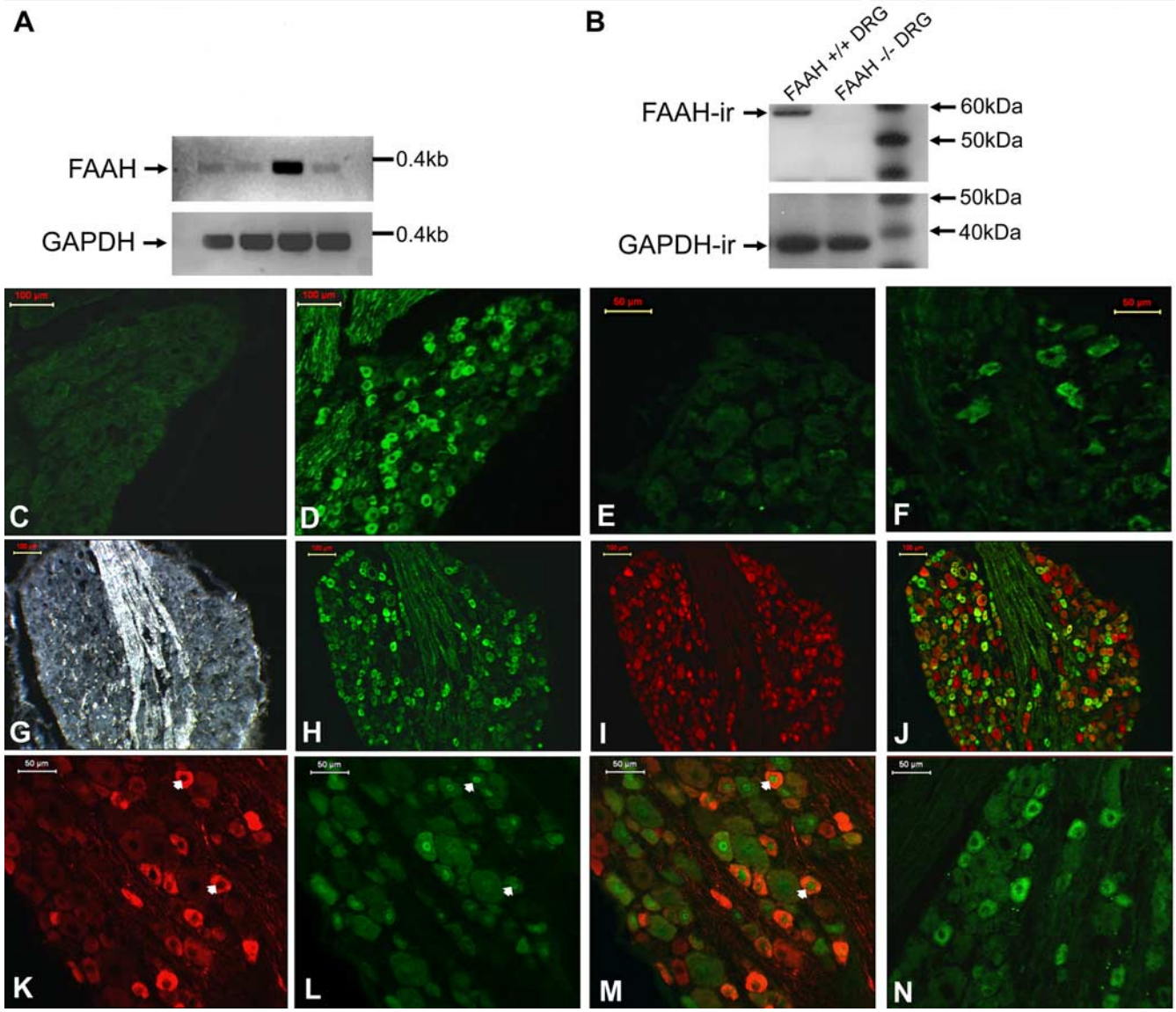

Figure 1. Localization of FAAH immunoreactivity in adult rodent DRG tissue. ***A***, Products of an RT-PCR reaction using primers for FAAH and GAPDH: mRNA samples extracted from two L4 rat DRG per lane; ~30 mg of rat hippocampus, ~30 mg of rat lumbar spinal cord. ***B***, Western blot analysis of FAAH immunoreactivity in DRG tissue from an $FAAH^{+/+}$ mouse. Immunoreactivity for FAAH is absent from $FAAH^{-/-}$ mouse DRG tissue. Reprobed immunoreactivity to GAPDH protein as the lane loading control. ***C–F***, ***N***, Antibody controls. ***C***, Adjacent rat DRG sections stained in the same run with preabsorbed ΔTM FAAH antibody (scale bar, 100 μm); or ***D***, non-preabsorbed ΔTM FAAH antibody (scale bar, 100 μm); ***E***, ΔTM FAAH antibody staining of fresh-fixed mouse DRG tissue from $FAAH^{-/-}$ mouse (scale bar, 50 μm); or ***F***, $FAAH^{+/+}$ mouse (scale bar, 50 μm). ***G–J***, Low-power micrograph images of adult rat L4 DRG (scale bars, 100 μm). ***G***, Dark-field image; ***H***, green immunofluorescent labeling of ΔTM FAAH-IR ganglion cells; ***I***, red immunolabeling of NeuN-IR neurons; ***J***, combined immunofluorescence labeling for ΔTM FAAH and NeuN. ***K–M***, High-power micrograph images (scale bars, 50 μm). ***K***, Arrows indicate ganglion cells with red immunofluorescent ΔTM FAAH labeling; ***L***, with green NeuN staining; and ***M***, colabeled with ΔTM FAAH and NeuN antibodies (yellow). ***N***, Comparable immunofluorescent labeling of L5 rat DRG cells using a FAAH antibody raised to a different immunogen (scale bar, 50 μm).

were analyzed by one-way ANOVA, with significance established by the Fisher's protected least significant difference (PLSD) test. Differences were regarded as significant at $p < 0.05$.

Results

FAAH mRNA is present in DRG tissue

First, we studied whether FAAH mRNA was expressed by primary sensory neurons in DRG. The PCR products generated using cDNA were prepared by reverse transcription from mRNA isolated from naive rat L4 DRG and corresponded to the size predicted for primers designed to amplify rat FAAH cDNA (394 bp) (Fig. 1*A*). Similar PCR products could be observed using samples prepared from rat hippocampus and spinal cord. Control samples, run in duplicated conditions but without the reverse-transcriptase enzyme, were negative (data not shown). This, together with the design of FAAH-specific primers across exon boundaries, excludes the possibility of contamination from genomic DNA and provides evidence for the expression of mRNA in rat lumbar DRG and spinal cord.

Specificity and selectivity of the anti-FAAH antibody

Next, to determine whether the antibody used to analyze FAAH expression was specific and selective and whether the FAAH mRNA in DRG was translated into protein, we ran a Western blot analysis of protein samples isolated from $FAAH^{+/+}$ and $FAAH^{-/-}$ mouse DRG, rat DRG, spinal cord, sciatic nerve, and hippocampus (Fig. 1*B*). In each sample (except for $FAAH^{-/-}$ mouse DRG), an immunoreactive band of ~60 kDa was detected by the ΔTM FAAH antibody, which is consistent with the pre-

dicted molecular mass of rat FAAH protein, ~63 kDa (Cravatt et al., 1996), and comparable with the size of FAAH-IR protein isolated from other neuronal tissues (Cravatt et al., 2001; Egertová et al., 2003). The same antibody, when used for immunohistochemistry, produced staining in a subpopulation of cells in sections of DRG taken from $FAAH^{+/+}$ mice (Fig. 1*F*). However, the staining was absent in DRG sections from $FAAH^{-/-}$ mice (Fig. 1*E*). DRG obtained from rats also contained a subpopulation of FAAH-IR cells (Fig. 1*G–J*,*K–M*). Colabeling of the sections with the NeuN marker of neuronal nuclei indicated that these FAAH-IR cells were primary sensory neurons (Fig. 1*J*,*M*). Preabsorption of the primary antibody resulted in a lack of FAAH immunoreactivity in rat DRG tissue (Fig. 1*C*) when compared with the staining produced using the non-preabsorbed antibody on a serial section from the same DRG (Fig. 1*D*). A similar staining pattern was observed in rat lumbar DRG tissue stained with an alternative FAAH antibody raised against a different area of the FAAH protein (Fig. 1*N*). These findings confirm the specificity of the FAAH antibody, as demonstrated previously for other types of neuronal tissue (Cravatt et al., 2001; Egertová et al., 2003), and suggest that FAAH mRNA is translated into protein in a subpopulation of primary sensory neurons in both mouse and rat DRG.

Localization of FAAH immunoreactivity in small DRG neurons

FAAH immunoreactivity was found in the cell soma of DRG neurons colabeled with NeuN (Fig. 1*J*,*M*). Of the 1804 NeuN-IR DRG cells captured for image analysis ($n = 6$), 591 were FAAH-IR. On average, 32.7 ± 0.8% (mean ± SEM) of NeuN-labeled cells sampled from each animal were FAAH-IR. The cell-size distribution of FAAH-IR and NeuN-IR neuron populations from L4 DRG revealed that most nucleated FAAH-IR neurons were small in size (Fig. 2*A*) compared with the total population of NeuN-IR neurons. The mean ± SEM area of FAAH-IR cells was 396.0 ± 5.6 μm^2. This was significantly smaller than the average size of NeuN-IR cells, 511.9 ± 8.4 μm^2 ($p < 0.05$, Kruskal–Wallis one-way ANOVA).

Distribution of FAAH among DRG neuron subpopulations

The location of FAAH immunoreactivity on small DRG neurons was confirmed by costaining studies with markers associated with small or large DRG cell populations (Fig. 2*B–F*). Considering only those neuronal profiles with a DAPI-stained nucleus, FAAH immunoreactivity demonstrated a high degree of colocalization with peripherin (neurofilament light), a marker found predominantly in small DRG neurons with unmyelinated C-fiber axons (Goldstein et al., 1991). On average, 85.6 ± 7.2% of FAAH-IR cells counted ($n = 180$) costained with peripherin antibodies and 48.6 ± 5.7% of peripherin-labeled cells ($n = 334$) stained with FAAH (Fig. 2*B*). In contrast, <2% of FAAH-IR neurons ($n = 131$) were colabeled with the NF200 antibody (Fig. 2*C*) recognizing the 200 kDa heavy chain neurofilament protein found in medium- to large-sized cell bodies subtending myelinated axons (Lawson and Waddell, 1991).

The population of DRG neurons with unmyelinated C-fibers can be further subdivided into cells that bind the lectin IB4 and those containing the neuropeptide CGRP (Snider and McMahon, 1998). FAAH immunoreactivity was predominantly found in the IB4-labeled subpopulation, as a larger proportion of FAAH-IR DRG cells colabeled with IB4 (72.0 ± 4.2%; $n = 131$) (Fig. 2*E*). A smaller proportion of DRG neurons were colabeled with FAAH and CGRP antibodies (39.4 ± 13.1%; $n = 76$), and only 30.1 ± 10.9% of CGRP-IR cells counted ($n = 244$) had FAAH labeling (Fig. 2*F*). Measurement of the average intensity of CGRP staining in FAAH-IR soma (74.4 ± 3.0 a.u.) showed that this was significantly lower than in CGRP-IR cells without FAAH staining (94.6 ± 2.0 a.u.; $p < 0.001$, *t* test). This indicates that a population of weakly CGRP stained neurons were FAAH-IR.

A large proportion of FAAH-IR neurons (64.5 ± 3.2%; $n = 124$) costained for TRPV1 (Fig. 2*D*), the receptor conferring capsaicin sensitivity on small nociceptive sensory neurons (Caterina et al., 1997). Analysis of costaining data produced using FAAH and TRPV1 antibodies indicates that approximately half of TRPV1-labeled cells do not have FAAH staining. Given that approximately half of the TRPV1-expressing cells are IB4 positive (Michael et al., 1999), and that FAAH was expressed mainly by IB4-labeled neurons, it is likely that the majority of neurons expressing TRPV1 and FAAH should also be IB4 positive.

Culturing does not induce major changes in FAAH expression in primary sensory neurons

Cultured adult rat DRG cells were costained with antibodies to FAAH and NF200 (Fig. 3*A*). On average, 26.3 ± 1.4% of $n = 437$ DRG cells were FAAH labeled. The NF200 antibody labeled 18.3 ± 1.5% of cells. In agreement with staining in DRG tissue sections, colabeling of FAAH with the NF200 large-cell marker was rare in cultured DRG cells (1.5 ± 1.2%). In addition, the average area of FAAH-IR cells (302.1 ± 16.9 μm^2; $n = 109$) was significantly smaller than NF200-labeled cells (650.9 ± 87.6 μm^2; $n = 68$; $p < 0.006$, Student's *t* test); cell-size distributions are shown in Figure 3*B*. The distribution of FAAH immunoreactivity within the small cell population of cultured rat DRG neurons is consistent with the pattern of labeling in tissue sections of rat DRG and with the costaining of FAAH immunoreactivity with a marker of small cells in cultured rat trigeminal neurons (Price et al., 2005). These data suggest that culturing does not induce major transcriptional or translational changes in FAAH expression.

FAAH is functional in primary sensory neurons

Next, we studied the effect the FAAH inhibitor URB597 on TRPV1-mediated responses in cultured primary sensory neurons after 2 d in culture. TRPV1 is a nonselective cationic channel, which, in addition to Na^+, K^+, and Ca^{2+}, is also permeable to Co^{2+} ions (Sathianathan et al., 2003; Singh Tahim et al., 2005). AEA is an endogenous agonist of the TRPV1 ion channel (Zygmunt et al., 1999), and incubation of cultured DRG neurons with AEA induces cobalt uptake in these cells (Singh Tahim et al., 2005). We assessed cobalt accumulation in cultured primary sensory neurons in a series of conditions, including the application of URB597, an inhibitor of FAAH that has been shown to reduce FAAH activity in cultured rat CNS tissue (Hohmann et al., 2005).

In control experiments, incubation of DRG neurons with capsaicin (1 μM) for 5 min in the presence of $CoCl_2$ induced Co^{2+} influx in a mean ± SEM of 32.1 ± 5.4% of cells ($n = 234$). The proportion of Co-ppt-positive cells was significantly higher than after incubating the cells with the $CoCl_2$-containing buffer without capsaicin (1.3 ± 0.4%; $n = 256$; $p < 0.05$, one-way ANOVA, followed by Fisher's PLSD test) (Fig. 3*D*). Incubation in $CoCl_2$ buffer containing either AEA (1 μM) or the FAAH inhibitor URB597 (1 μM) also induced Co^{2+} influx (Fig. 3*C*). The proportion of Co-ppt-positive cells after AEA or URB597 treatment was 8.3 ± 3.8%, $n = 175$ and 8.6 ± 2.2%, $n = 189$, respectively (not significantly different from the control). Preincubation and coincubation of cells with URB597 (1 μM) added together with AEA

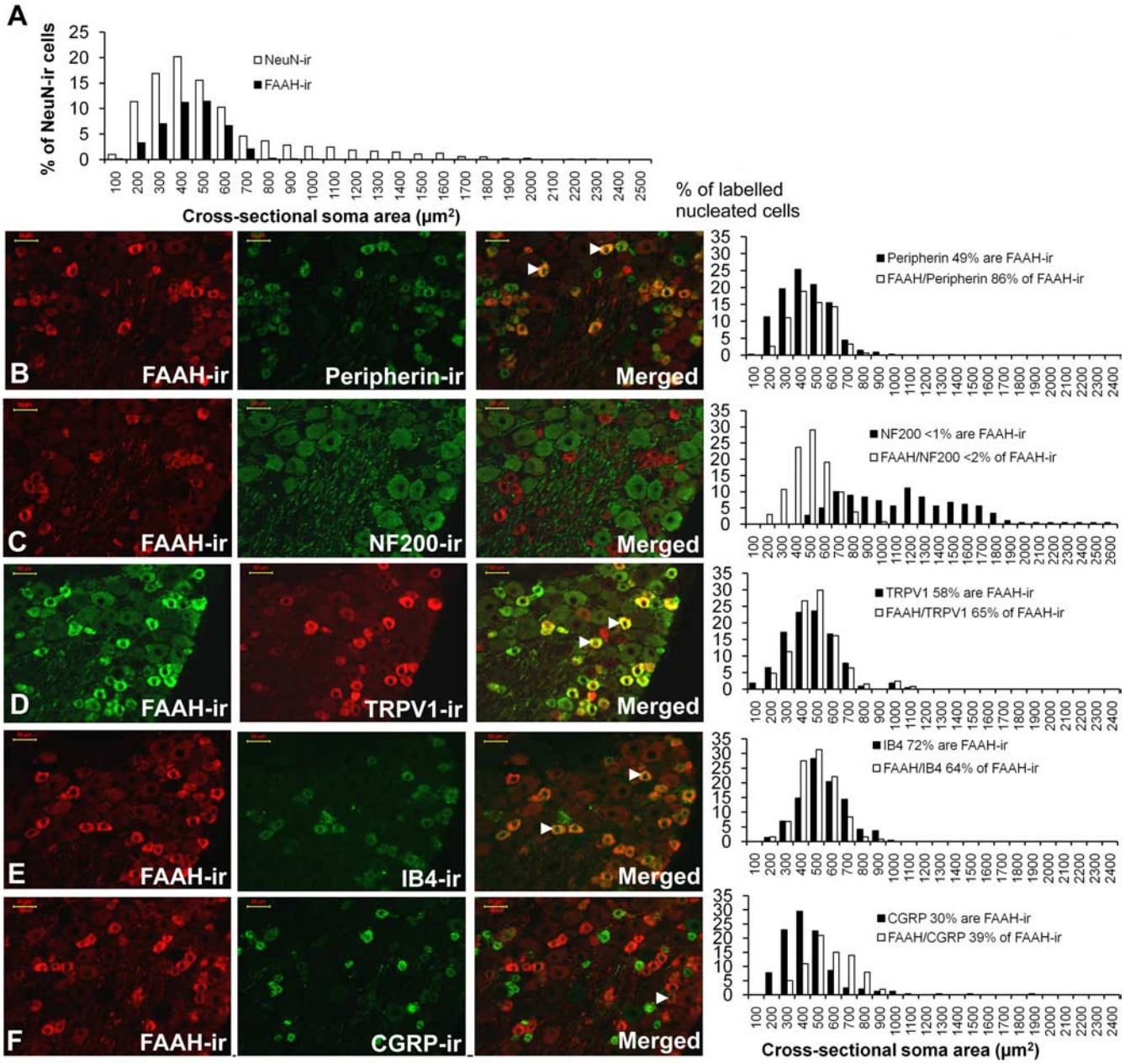

Figure 2. Cell-size analysis of FAAH-IR DRG neurons. ***A***, Cell-size distribution of 1804 NeuN-IR neurons sampled from adult rat L4 DRG tissue (white columns). Left-shifted cell-size distribution of FAAH-IR neurons within this population (black columns) indicating that FAAH-IR neurons most frequently have small soma areas ($<600\ \mu m^2$). ***B–F***, Double staining of FAAH with markers of neuronal subpopulations in rat L4 DRG tissue (white arrows indicate yellow-colored colabeled cells in the merged image) adjacent to the cell-size distribution of marker-positive cells and those colabeled with FAAH: ***B***, peripherin; ***C***, NF200; ***D***, TRPV1; ***E***, IB4; ***F***, CGRP. Scale bars, 50 μm.

in the $CoCl_2$ buffer produced a significant increase in the proportion of cells positive for Co-ppt but not when the TRPV1 receptor antagonist capsazepine (10 μM) was added to both the pretreatment and $CoCl_2$-containing buffers ($p < 0.05$, one-way ANOVA, Fisher's PLSD test) (Fig. 3*D*). The proportion of cells positive for Co-ppt after treatment with 1 μM AEA or 1 μM URB597 also reached significance over the control when these agents were applied in the presence of the CB_1 receptor antagonist SR141716 (12.6 ± 4.6%, $n = 203$ with 1 μM SR141716 and 1 μM AEA, and 12.7 ± 3.5%, $n = 185$ with 1 μM SR141716 and 1 μM URB597 treatment) ($p < 0.05$, one-way ANOVA, Fisher's PLSD test) (Fig. 3*D*).

Localization of FAAH immunoreactivity in spinal cord and sciatic nerve

In addition to DRG, FAAH protein was also detected in samples from rat spinal cord and sciatic nerve by Western blotting (Fig. 4*A*). Thus, we studied whether FAAH expression in those structures was attributable to transport of this protein to the peripheral and central terminals of primary sensory neurons. FAAH immunostaining was observed in transverse sections of rat lumbar spinal cord both in the white and gray matter of both the dorsal and ventral horns (Fig. 4*B*). In colabeling experiments, circular areas of FAAH immunoreactivity in the gray matter of dorsal and ventral horns were associated with NeuN labeling,

indicating that FAAH immunoreactivity was located within the soma and dendrites of neurons (Fig. 4*Bii–Biv*). The presence of FAAH-IR neurons in the spinal cord is consistent with previous observations (Tsou et al., 1998; Romero et al., 2002). Double staining with antibodies to CB_1 and FAAH revealed a regional codistribution of punctate CB_1 labeling and FAAH-IR neurons in the upper laminae of the dorsal horn (Fig. 4*Ci*,*Cii*). Intense immunofluorescent labeling of the CB_1 receptor was also observed within the dorsal lateral funiculus, again consistent with previous observations by Farquhar-Smith et al. (2000), and this was located surrounding nucleated cells stained with the FAAH antibody (Fig. 4*Civ*).

In agreement with the FAAH expression observed by Western blotting, FAAH immunoreactivity was also observed in longitudinal sections of sciatic nerve tissue, with intense staining present in discreet areas along fiber tracts and weaker staining present in longitudinal fibers (Fig. 4*Di*,*Ei*). Costaining with the S100 antibody (marker of Schwann cells) (Fig. 4*Diii*,*Div*,*Eiii*,*Eiv*) revealed colocalization of FAAH and S100 in nucleated, cell-like structures that remained separate from nerve fibers labeled with NF200 (Fig. 4*Fi*). Staining of nerve tissue in cross section confirmed FAAH labeling of structures surrounding nerve fibers. FAAH was only present in fibers that were labeled with the S100 antibody (Fig. 4*Fiv*). To investigate evidence for axonal transport of FAAH-IR material in DRG neurons, FAAH staining was also performed on longitudinal sections of sciatic nerve, harvested at either 24 h or 7 d after an axotomy injury. There was no visible accumulation of FAAH immunoreactivity proximal to the injury site at either time point, which indicates that FAAH is not targeted to the axons of DRG neurons.

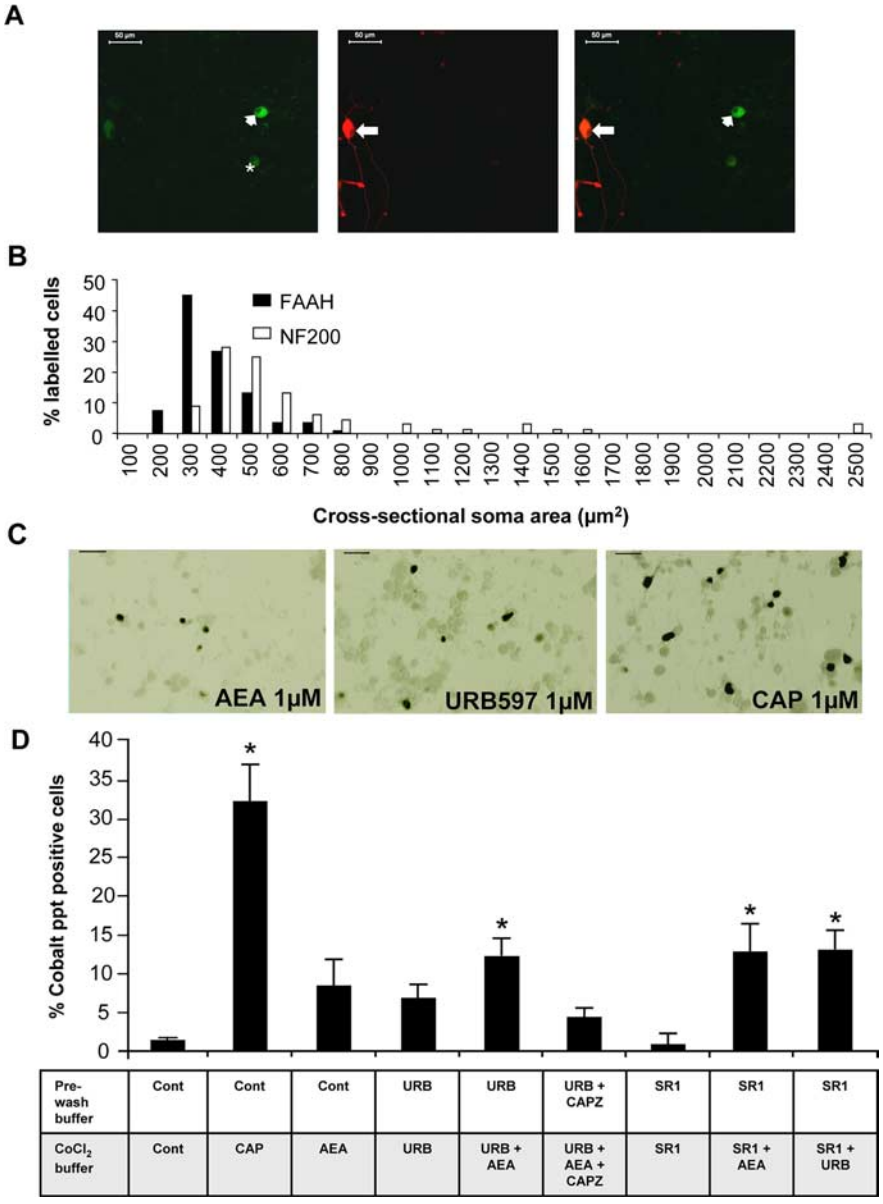

Figure 3. Localization of FAAH immunoreactivity in cultured DRG neurons, cell-size analysis, and cobalt uptake experiments. ***A***, Immunofluorescent images of cultured adult rat DRG neurons (scale bars, 50 μm). Left, FAAH-IR cell (arrowhead), unlabeled cell (asterisk). Middle, NF200-IR cell (block arrow). Right, Merged image shows no overlap of FAAH-IR and NF200-IR cells. ***B***, Size distribution of FAAH-IR and NF200-IR cultured adult rat DRG neurons (437 cells sampled, $n = 4$). ***C***, Micrograph images of cultured adult rat DRG neurons after precipitation of cobalt chloride (scale bars, 50 μm). Dark-colored cells contain cobalt precipitate after a cobalt uptake experiment with the treatment indicated. ***D***, Cobalt uptake experiments: mean percentage of cultured adult rat DRG neuronal cells with an optical density above the threshold positive for Co-ppt after the treatments indicated in the corresponding table below each graph column ($n = 3–6$ experiments per group). Preincubation of cultures was performed for 5 min with control buffer (Cont) alone or with one of the following solutions added: URB597 (URB) at 1 μM with or without capsazepine (CAPZ) at 10 μM or SR141617 (SR1) at 1 μM (see Table 1). Cells were then incubated for 5 min with a buffer containing $CoCl_2$ together with other solutions according to the table. The proportion of cells positive for Co-ppt was significantly higher than control levels after treatment with capsaicin at 1 μM. Treatment with AEA at 1 μM produced a significant increase in cells positive for Co-ppt only after pretreatment and cotreatment with the FAAH inhibitor URB597 at 1 μM but not if this experiment was performed in the presence of CAPZ. Pretreatment and cotreatment with the CB_1 receptor inhibitor SR141617 at 1 μM also produced significant increases in the proportion of Co-ppt-positive cells in response to either AEA at 1 μM or URB597 at 1 μM added to the $CoCl_2$ buffer. $^*p < 0.05$, one-way ANOVA, Fisher's PLSD test.

Injury to peripheral nerves induces changes in FAAH expression pattern in DRG

Nerve injury induces transcriptional, translational, and posttranslational changes in primary sensory neurons (Hökfelt et al., 1994; Noguchi et al., 1995). It is believed that at least some of these changes might have causal relationship with the development of pain associated with injuries of peripheral nerves. Thus, next we studied the effect of nerve injury on FAAH expression in primary sensory neurons in two animal models.

Axotomy

Seven days after unilateral axotomy or sham injury to the sciatic nerve, L5 DRG were harvested and processed for FAAH immunohistochemistry. A change in the size of FAAH-IR neurons was observed on DRG sections that were ipsilateral to the axotomy injury (Fig. 5). FAAH staining was now observed within the soma of medium- to large-sized DRG neurons on the ipsilateral side to axotomy (Fig. 5*A*), whereas only small-sized neurons on the con-

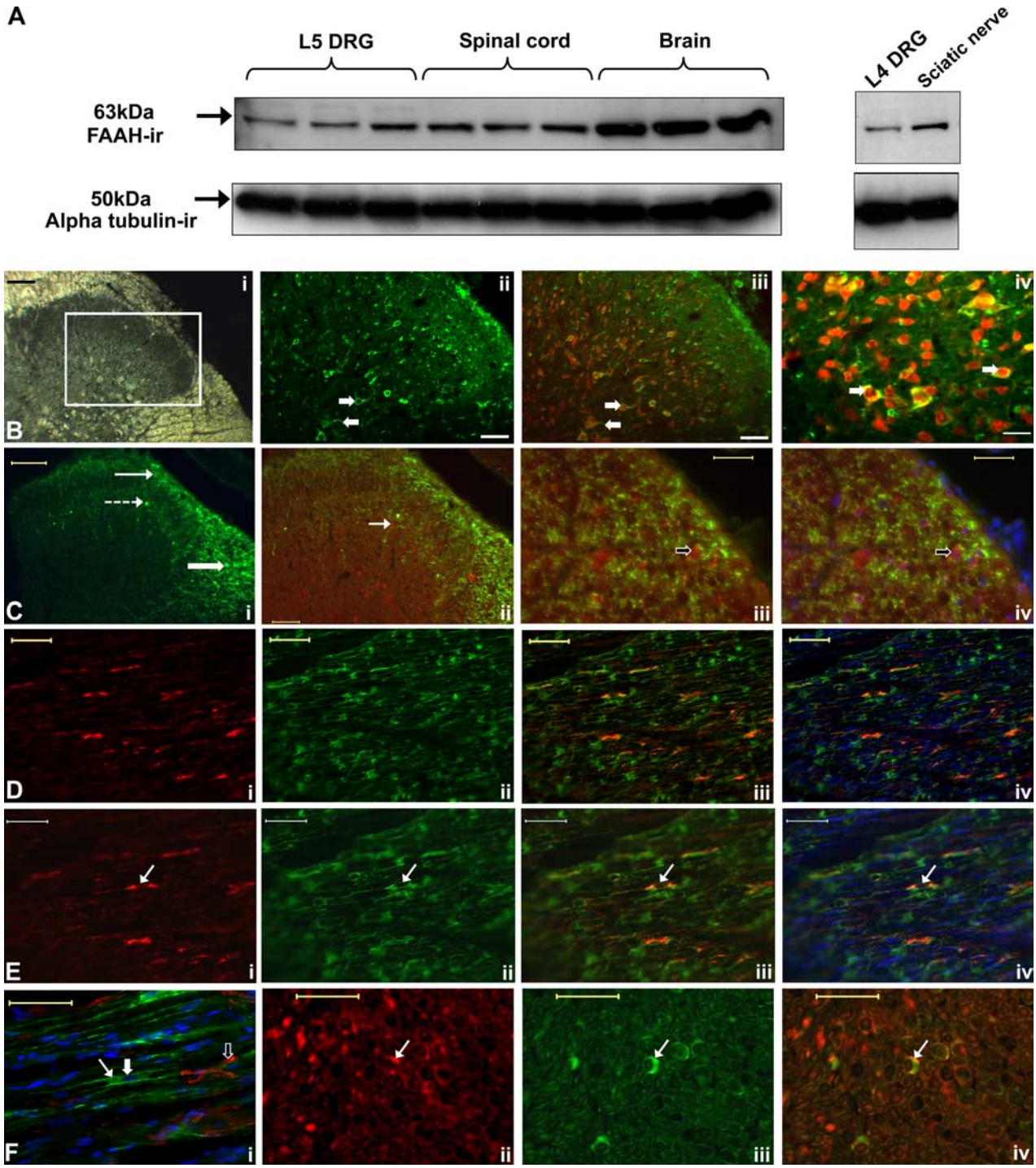

Figure 4. Localization of FAAH immunoreactive in adult rat spinal cord and sciatic nerve tissue. ***A***, Western blot showing FAAH-IR bands for replicate samples of L5 DRG, spinal cord, and brain tissue. Separate blot showing FAAH-IR samples from sciatic nerve run alongside L4 DRG. α-Tubulin immunoreactivity is shown as a lane loading control. ***B***, ***C***, Immunofluorescent staining of adult rat lumbar spinal cord tissue. ***Bi***, Dark-field orientation image of the dorsal horn: white box indicates area stained in image ***Bii***. ***Bii***, Confocal image showing FAAH labeling (green) of soma and dendrite-like structures (block arrows). Scale bar, 50 μm. ***Biii***, Colabeling of FAAH-IR structures with NeuN (red). Scale bar, 50 μm. ***Biv***, Colabeling of FAAH immunoreactivity and NeuN immunoreactivity in ventral horn motor neurons (block arrows). Scale bar, 50 μm. ***Ci***, CB_1 staining in the dorsal horn (green): punctate labeling of lamina I (line arrow), Iii/i border (dotted arrow), and lateral spinal nucleus (block arrow). Scale bar, 100 μm. ***Cii***, Regional colocalization of FAAH-IR (red) soma (arrow) and CB_1 immunoreactivity (green) in the upper dorsal horn. Scale bar, 50 μm. ***Ciii***, High-power image of the lateral spinal nucleus: FAAH-labeled cell (red) (block arrow) surrounded by punctuate CB_1 labeling (green). Scale bar, 30 μm. ***Civ***, Same image in ***Ciii*** but showing additional DAPI nuclear staining (blue) identifying the soma of an FAAH-IR (red) cell (block arrow). Scale bar, 30 μm. ***D–F***, Immunofluorescent staining of sciatic nerve tissue. ***D***, Low-power images. ***Di***, FAAH staining (red) on a longitudinal section of rat sciatic nerve tissue. ***Dii***, Image of the same field showing double labeling with S100 antibodies (green). ***Diii***, Image of the same field showing merged image of S100 and FAAH labeling together with triple labeling with NF200 antibodies (blue). Scale bars, 50 μm. ***E***, Higher-power images. ***Ei***, An FAAH-IR cell (arrow) on a longitudinal section of sciatic nerve tissue. ***Eii***, Image of the same field showing labeling of the same cell with S100 antibodies (green). ***Eiii***, Image of the same cell showing merged image of S100 and FAAH labeling together with triple labeling with NF200 antibodies (blue). Scale bars, 30 μm. ***Fi***, High-power longitudinal section of sciatic nerve showing FAAH-IR labeling (green) of a cell (white arrow) containing a DAPI-stained (blue) nucleus (white block arrow). Separate labeling of neurofilament with NF200 antibodies (red) (black block arrow). ***Fii–Fiv***, Cross-sectional images of mouse sciatic nerve. ***Fii***, Red FAAH labeling of structures surrounding nerve filaments (arrow). ***Fiii***, Green S100 labeling of Schwann cells surrounding nerve filaments (arrow). ***Fiv***, Merged image of S100 and FAAH labeling indicating areas of label overlap (arrow). Scale bars, 30 μm.

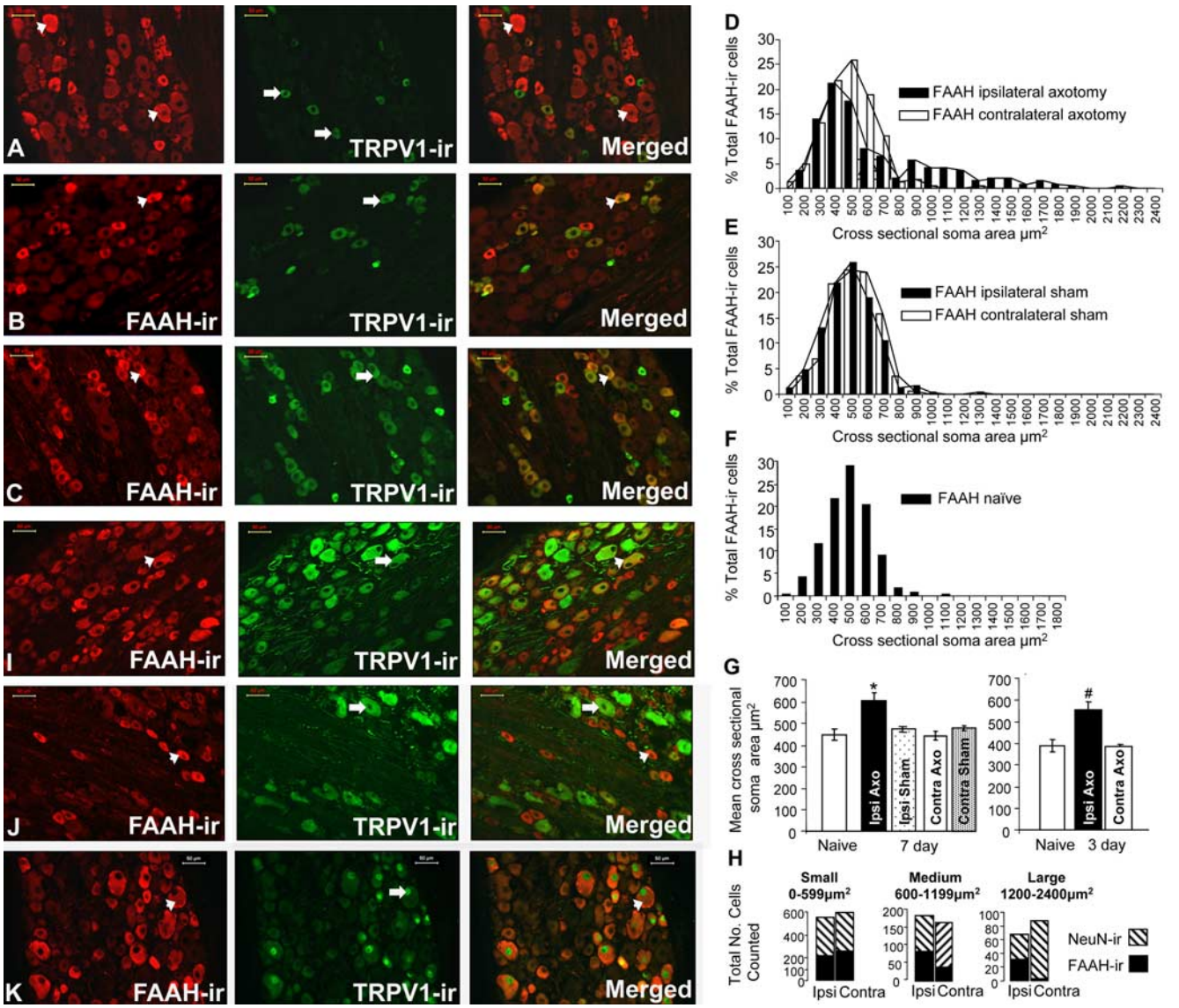

Figure 5. Larger-sized DRG neurons are FAAH-IR after axotomy injury to the sciatic nerve. ***A***, ***B***, ***I–K***, Immunofluorescent labeling of L5 DRG tissue 7 d after an axotomy injury to the sciatic nerve (scale bars, 50 μm). ***A***, DRG tissue ipsilateral to the injury. Left, Large-sized FAAH-IR neurons (arrows). Middle, Small-sized TPRV1-IR neurons (block arrows). Right, Merged image; large-sized FAAH-IR neurons (arrows) are not TRPV1 labeled. ***B***, Same animal as in ***A***, DRG tissue contralateral to the injury. Left, Small-sized FAAH-IR neuron (arrow). Middle, Small TRPV1-IR neuron (block arrow). Right, Colabeling of TRPV1 and FAAH in a small neuron (arrow). ***C***, L5 DRG tissue ipsilateral to a sham axotomy injury. Left, Small-sized FAAH-IR neuron (arrow). Middle, Small TRPV1-IR neuron (block arrow). Right, Small neuron colabeled with TRPV1 and FAAH immunoreactivity (arrow). ***D***, Cell-size distribution of FAAH-IR L5 DRG neurons on the ipsilateral and contralateral side to a 7 d axotomy injury: rightward shift in the size of FAAH-IR neurons on the ipsilateral side to injury (total of 1656 NeuN-labeled cells sampled, $n = 6$). ***E***, Cell-size distribution of FAAH-IR L5 DRG neurons on the ipsilateral and contralateral side to a 7 d sham axotomy injury: comparable cell-size distribution of FAAH-IR neurons on the ipsilateral and contralateral sides to sham injury (total of 952 NeuN-labeled cells sampled, $n = 4$). ***F***, Cell-size distribution of FAAH-IR L5 DRG neurons from naive animals (total of 1241 NeuN-labeled cells sampled, $n = 4$). ***G***, Mean cell-area plot for FAAH-IR neurons from axotomized ($n = 6$) or sham axotomized ($n = 4$) and naive ($n = 4$) animals at 7 d postoperation (PO). PO7, FAAH-IR neurons on the ipsilateral side to injury are larger than on the contralateral side or the ipsilateral side of sham-injured or naive animals. $^{*}p < 0.05$, ANOVA with *post hoc* Tukey's test. Area plots for ipsilateral and contralateral FAAH-IR neurons from axotomized animals ($n = 3$) 3 d after operation and naive animals ($n = 4$). PO3, FAAH-IR neurons on the ipsilateral side are larger than the contralateral side or naive animals. $^{\#}p < 0.05$, Student's *t* test. ***H***, Plot of the number of L5 DRG cells measured in ***D*** in each size category on ipsilateral and contralateral sides to 7 d axotomy injury. ***I***, DRG tissue ipsilateral to axotomy. Left, Large FAAH-IR neuron (arrow). Middle, NF200 labeling of a large-sized neuron (block arrow). Right, Merged image showing FAAH and NF200 colabeling in a large-sized neuron (arrow). Scale bars, 50 μm. ***J***, Same animal as in ***I***, contralateral to axotomy. Left, Small FAAH-IR neuron (arrow). Middle, NF200 labeling of large-sized neuron (block arrow). Right, FAAH (arrow) and NF200 labeling (block arrow) are not colocalized in the merged image. Scale bars, 50 μm. ***K***, DRG tissue ipsilateral to axotomy. Left, Large FAAH-IR neuron (arrow). Middle, ATF3 labeling in a large-sized neuron (block arrow). Right, ATF3 labeling within a large-sized FAAH-IR neuron (arrow). Scale bars, 50 μm.

tralateral side were FAAH-IR (Fig. 5*B*), consistent with the pattern of staining found in lumbar DRG from naive animals (Fig. 1*K*). This difference in the size of FAAH-IR neurons on the ipsilateral compared with the contralateral side to injury was not observed in DRG tissue from sham-operated animals (Fig. 5*C*). Cell-size analysis of DRG soma derived from the ipsilateral and contralateral sides of axotomized or sham-operated rats 7 d after surgery and naive rats (Fig. 5*D–F*) confirmed a rightward shift in the size of FAAH-IR neurons on the injured side of axotomized rats compared with those on the contralateral side (Fig. 5*D*). The mean area of the FAAH-IR DRG neurons was significantly increased on the side ipsilateral to an axotomy injury (603.3 $\pm$ 38.4 μm^2; $n = 6$; 330 cells) compared with FAAH-IR neurons from the uninjured side (440.5 $\pm$ 20.7 μm^2; $n = 6$; 448 cells; $p < 0.05$

ANOVA, *post hoc* Tukey's test) and those on the ipsilateral side to sham-operated animals (Fig. 5*G*). This change could not be accounted for by differences in the number of NeuN-labeled neurons sampled from ipsilateral (total of $n = 808$ cells) and contralateral (total of $n = 848$ cells) DRG in each size category (Fig. 5*H*) and did not occur in DRG profiles from the injured and uninjured sides of sham-operated or naive animals (Fig. 5*E–G*). The increase in the average size of FAAH-IR neurons ipsilateral versus contralateral to injury was also significant when DRG tissue was harvested 3 d after axotomy surgery (Fig. 5*G*). The proportion of FAAH-IR neurons on the ipsilateral side to injury was 42.1 ± 5.7% ($n = 808$ NeuN-IR cells) compared with the contralateral side (35.7 ± 3.2%; $n = 848$ NeuN-IR cells), although this difference was not statistically significant. The proportion of FAAH-IR cells on the contralateral side was close to that found in naive animals (32.8 ± 0.9%; $n = 1241$ NeuN-IR cells).

The change in the distribution pattern of FAAH immunoreactivity was confirmed by costaining of large FAAH-IR cells with anti-NF200 antibodies ipsilateral, but not contralateral, to an axotomy injury (Fig. 5*I*,*J*). Costaining the sections with the anti-FAAH and anti-TRPV1 antibodies was also performed on both ipsilateral and contralateral DRG sections after axotomy (Fig. 5*A*,*B*). In agreement with previous findings (Michael and Priestley, 1999), these experiments showed that the proportion of TRPV1-IR DRG neurons ipsilateral to axotomy injury (14.5 ± 1.9%; $n = 386$) was reduced compared with the proportion of these cells on the contralateral side (38.4 ± 3.7%; $n = 409$). Consistent with the changes in FAAH and TRPV1 expression, the relative number of cells coexpressing FAAH and TRPV1 was also altered. Whereas 60.7 ± 10.6% ($n = 131$) of the FAAH-IR cells were colabeled with TRPV1 on the contralateral side, only 8.5 ± 3.9% ($n = 164$) of the FAAH-labeled cells costained for TRPV1 on the ipsilateral side. The difference in the proportion of the cells between the two sides was significant ($p < 0.0001$). Costaining was also performed using the anti-FAAH antibody and an antibody raised against ATF3 (Fig. 5*K*), which identifies primary sensory neurons under sustained cellular stress. There were no ATF3-immunolabeled cells on the contralateral side, but the majority (74.9 ± 3.5; $n = 282$) of FAAH-IR neurons ipsilateral to axotomy injury contained ATF3 labeling, including large-sized neurons of $>600\ \mu m^2$.

Spinal nerve transection

In agreement with previously published data, after the ligation and transection of a lumbar spinal nerve (SNT injury), animals developed reflex hypersensitivity to mechanical and cold stimuli, assessed 7 d after surgery. The mean ± SEM force in grams required for reflex withdrawal of injured hindpaws (26.9 ± 4.0 g) was significantly lower when compared with the preinjury paw baseline (52.9 ± 2.3 g) ($p < 0.001$) and with the responses of uninjured contralateral paws (48.8 ± 1.7 g) ($p < 0.001$) or of the ipsilateral paws of sham-operated animals (45.4 ± 2.5 g) ($p < 0.01$; ANOVA, Tukey's tests; $n = 4$ per group). In sham-operated animals, no differences were found between mean withdrawal responses at baseline (48.5 ± 2.1 and 49.8 ± 2.1 g) and 7 d after injury (45.4 ± 2.5 and 50.0 ± 2.6 g) for ipsilateral and contralateral paws, respectively, and there was no difference in baseline responses (50.6 ± 2.5 g) compared with 7 d after injury on the contralateral side of SNT animals ($p > 0.05$; ANOVA, Tukey's test). SNT-injured paws all responded with 100% frequency to a cold acetone stimulus, a significantly higher response rate compared with the opposite uninjured paws (mean response rate, 5.0 ± 5.8%), the ipsilateral paws of sham-operated animals (10.0 ± 6.7%), and ipsilateral pre-SNT injury baseline (0%) ($p < 0.001$, Kruskal–Wallis ANOVA, Student–Newman–Keuls; $n = 4$ per group). Using this test, there was no difference in the responses of sham-operated animals on the ipsilateral side versus the contralateral side to injury (5.0 ± 5.8%) or from respective preinjury baselines (0 and 5.0 ± 5.8%).

As with DRG tissue from axotomized animals, larger-sized neurons ipsilateral to the SNT injury stained positively for FAAH immunoreactivity (Fig. 6*A*), whereas those on the contralateral side (Fig. 6*B*) and the ipsilateral side of sham-operated animals did not (Fig. 6*C*). Cell-size analysis confirmed a pronounced rightward shift in the size distribution of ipsilateral FAAH-IR neurons (Fig. 6*D*). On average, FAAH-IR cells were significantly larger ipsilaterally (658.1 ± 12.1 μm^2; $n = 219$) than those on the contralateral side (402.4 ± 12.4 μm^2; $n = 156$) or on the ipsilateral or contralateral side of sham-operated animals (414.5 ± 10.7 μm^2, $n = 215$ and 429.2 ± 12.4, $n = 224$ for ipsilateral and contralateral sides, respectively) (Fig. 6*E*). SNT injury increased the proportion of FAAH-IR cells (50.6 ± 3.7%; $n = 442$ NeuN-IR cells) when compared with the contralateral side (34.5 ± 5.8%; $n = 449$ NeuN-IR cells) or the ipsilateral side of sham-operated animals (33.8 ± 3.1%; $n = 630$) ($p < 0.05$, ANOVA, Tukey's test), whereas the proportion of FAAH-IR neurons on the contralateral side of SNT animals was not significantly different from that found in naive animals (32.7 ± 0.8%; $n = 1402$ NeuN-IR cells). There was a concomitant reduction in the proportion of TRPV1-labeled cells on the injured side (1.6 ± 1.9%; $n = 4$) compared with the uninjured side (46.1 ± 1.3%; $n = 162$) (Fig. 6*A*,*B*). This ipsilateral decrease was more extensive compared with axotomized tissue ($p < 0.05$, ANOVA, Tukey's test).

Western blot analysis of protein extracts from SNT-injured and contralateral DRG confirmed that FAAH immunoreactivity was upregulated on the ipsilateral side of the injury (Fig. 6*F*). Densiometric analysis of the FAAH-IR bands showed higher optical density values with ipsilateral DRG samples compared with those on the uninjured, contralateral side. There was no difference in the optical density values measured for GAPDH-IR bands (Fig. 6*G*).

Inflammation of peripheral tissues does not induce changes in FAAH expression pattern

Similarly to peripheral nerve injury, inflammation of the peripheral tissues also induces plastic changes to cell markers in primary sensory neurons (Calzà et al., 1998; Ji et al., 2002). Thus, we also studied whether inflammation of peripheral tissues induces any changes in the FAAH expression pattern. CFA injection induced inflammation of the hindpaw skin and produced concomitant reflex hypersensitivity to thermal and mechanical stimuli, measured by behavioral testing before and after injection. Withdrawal latencies to thermal stimulation were significantly shorter for the inflamed hindpaw compared with preinjury baseline levels and were also shorter when compared with the uninjured contralateral paw ($p < 0.05$, one-way ANOVA, Tukey's test) (Fig. 7*A*). Similarly, the threshold for paw-withdrawal responses to mechanical stimulation were also significantly reduced ipsilaterally at 1 and 2 d after CFA injection when compared with preinjury baseline levels and the responses of the contralateral paws at these time points ($p < 0.01$, one-way ANOVA, Tukey's test) (Fig. 7*B*). Ipsilateral and contralateral L5 DRG from CFA-treated animals ($n = 4$) were processed for FAAH immunohistochemistry. Analysis of the cell-size distribution of FAAH-IR soma (Fig. 7*C*) revealed no inflammation-related changes ipsilateral to CFA injection. There was no difference in the mean ± SEM soma size

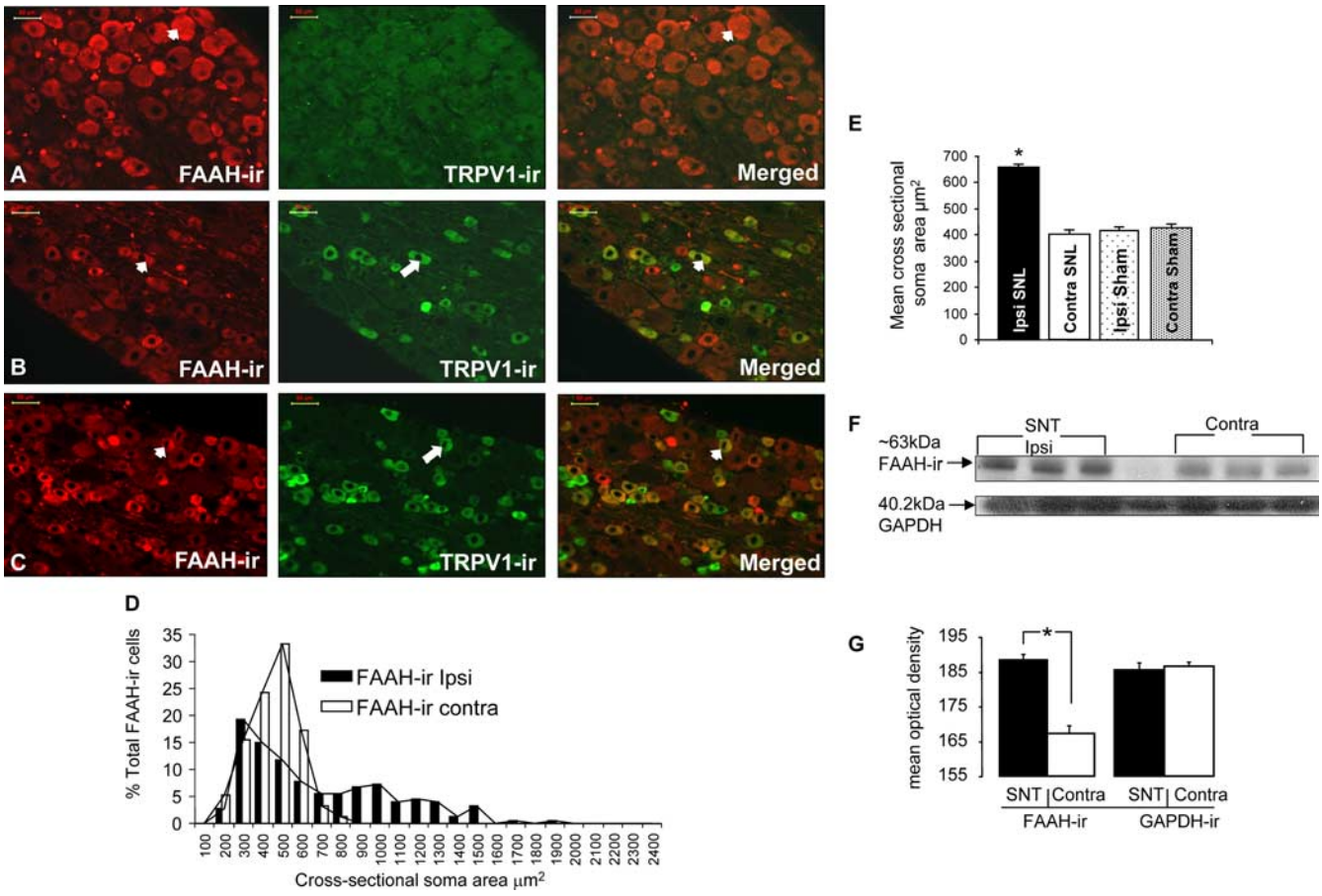

Figure 6. Larger-sized DRG neurons are FAAH-IR after SNT. Immunolabeling of lumbar DRG tissue from rats receiving a spinal nerve transection injury. Left, FAAH labeling. Middle, TRPV1 labeling. Right, Neurons with TRPV1 and FAAH labeling (scale, bars 50 μm). ***A***, Images of DRG tissue on the ipsilateral side to SNT injury. Left, A large-sized FAAH-IR neuron (arrow). Middle, No TRPV1-labeled cells visible after TRPV1 staining. Right, FAAH-IR large-sized neuron (arrow); no cells colabeled with FAAH and TRPV1. ***B***, Images of DRG tissue on the contralateral side to SNT injury of the same animal as in ***A***. Left, Small FAAH-IR neuron (arrow). Middle, Small TRPV1-IR neuron (block arrow). Right, Neuron colabeled with TRPV1 and FAAH (arrow) immunoreactivity. ***C***, Images of lumbar DRG tissue from the ipsilateral side of a sham-operated SNT animal. Left, Small FAAH-IR neuron (arrow). Middle, Small TRPV1-IR neuron (block arrow). Right, Colabeled TRPV1-IR and FAAH-IR neuron (arrow). ***D***, Cell-size distribution of FAAH-IR neurons ipsilateral and contralateral to an SNT injury. ***E***, Mean cell area plot for FAAH-IR neurons on the ipsilateral and contralateral sides of SNT-injured animals ($n = 4$) and sham-operated animals ($n = 4$). The size of FAAH-IR DRG neurons is greater ipsilateral to an SNT injury compared with the contralateral side and the ipsilateral and contralateral sides of sham-operated animals (*$p < 0.001$, one-way ANOVA, *post hoc* Tukey's test). ***F***, Western blot of lumbar DRG tissue samples ipsilateral and contralateral to SNT injury. Each sample contained tissue from two DRG (total of $n = 6$). ***G***, Optical density measurements (mean ± SEM) of FAAH-IR and GAPDH-IR Western blot bands from lumbar DRG samples ipsilateral and contralateral to spinal nerve transection injury (average of 3 separate gels). Mean optical density measurements for Western blot bands of FAAH immunoreactivity were higher ipsilateral to the injury compared with the contralateral side (*$p < 0.05$, one-way ANOVA, Tukey's test); there was no ipsilateral versus contralateral difference in the optical densities of GAPDH-IR bands.

of FAAH-IR DRG neurons on the inflamed side compared with the contralateral side or DRG neurons from naive animals ($p = 0.885$, one-way ANOVA). There was also no change in the average proportion of FAAH-IR DRG neurons ipsilateral (27.2 ± 3.1%; $n = 467$ nucleated cells) versus contralateral (29.2 ± 1.7%; $n = 446$ nucleated cells) to the inflammation ($p = 0.5921$, Student's t test).

Discussion

To better understand how AEA might modulate peripheral nociceptive transmission, it is important to map the location of FAAH in tissue relevant to this function. This study investigated FAAH expression in DRG sensory neurons, peripheral nerve tissue, and spinal cord neurons.

RT-PCR experiments provided evidence for the presence of FAAH mRNA in adult rat DRG and spinal cord. FAAH protein was detected in rat DRG, spinal cord, and peripheral nerve tissue using Western blotting. The size of the immunoreactive bands was comparable with those obtained from brain tissue homogenate (Egertová et al., 1998; Cravatt et al., 2001; Ortega-Gutiérrez et al., 2004) and cells transfected with FAAH cDNA (Patricelli et al., 1998).

FAAH protein-specific antibodies labeled approximately one-third of neuronal soma in rat DRG tissue and dissociated culture. Cell-size measurements and the absence of costaining with NF200 antibodies indicated that FAAH-IR DRG neurons were small, of the kind subtending unmyelinated C-fiber axons (Lawson and Waddell, 1991) and colocalizing with small cell markers: peripherin, IB4, and TRPV1 (Goldstein et al., 1991; Michael and Priestley, 1999; Liu et al., 2004). Many FAAH-IR neurons (64.5%) costained for TRPV1, consistent with FAAH and TRPV1 costaining observed in cultured rat trigeminal ganglia neurons (Price et al., 2005) and hippocampal and cerebellar mouse brain neurons (Cristino et al., 2008).

Colocalization of FAAH and TRPV1 in DRG soma is supported by functional evidence from cobalt uptake experiments. Pretreatment of DRG cultures with the FAAH enzyme inhibitor URB597 increased the proportion of cells positive for Co-ppt after AEA application. AEA- and URB597-dependent cobalt up-

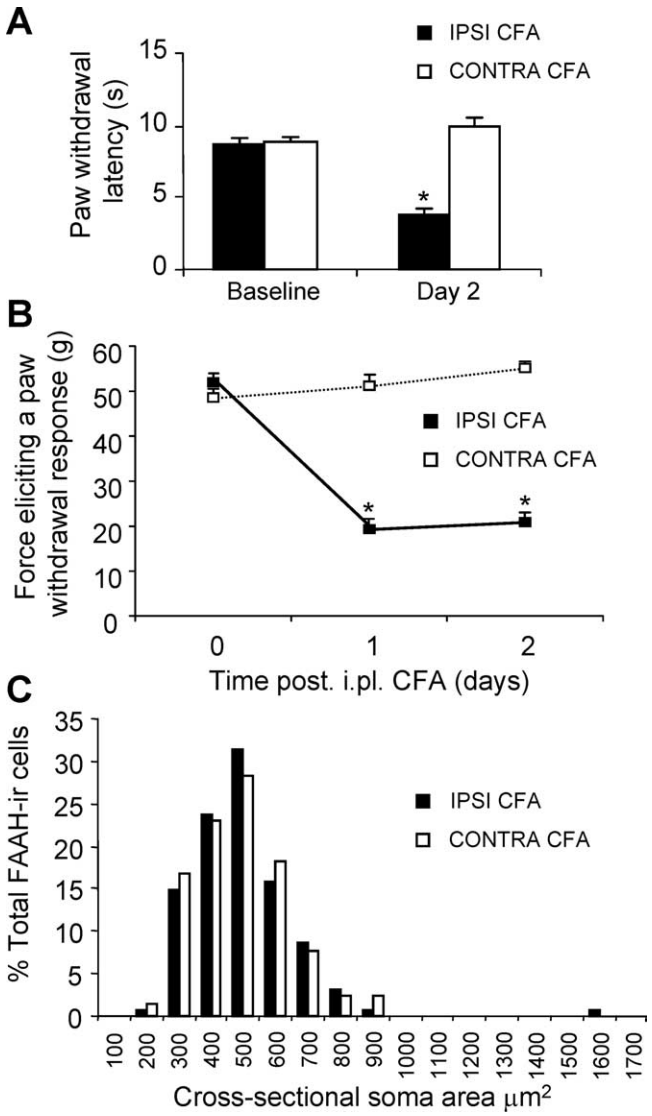

Figure 7. CFA inflammation. Behavior and cell-size analysis of FAAH-IR DRG neurons. ***A***, At 2 d after CFA injection, paw-withdrawal latencies to a heat stimulus (mean ± SEM), measured using the plantar test in CFA-inflamed rat hindpaws, were shorter than baseline withdrawal latencies and those for the noninflamed contralateral paws (*$p < 0.05$, one-way ANOVA, Tukey's test). ***B***, Paw-withdrawal latencies to a mechanical stimulus (mean ± SEM), measured using an electronic von Frey device in CFA-inflamed rat hindpaws, were lower compared with preinjury baseline values and those of noninflamed contralateral paws tested at 1 and 2 d after CFA intraplantar (i.pl.) injection (*$p < 0.01$, one-way ANOVA, Tukey's test). ***C***, Cell-size distribution of FAAH-IR DRG neurons ipsilateral and contralateral to a CFA inflammation of the rat hindpaw, 2 d after CFA injection. There was no difference in the mean ± SEM soma size of FAAH-IR DRG neurons on the inflamed side ($n = 127$) compared with the contralateral side ($n = 131$) or DRG neurons from naive animals ($n = 143$) ($p = 0.885$, one-way ANOVA).

take was blocked by pretreatment with the TRPV1 receptor antagonist capsazepine. These results suggest that FAAH inhibition raises the concentration of AEA inside DRG cells, which increases TRPV1 activation and the influx of cobalt ions.

AEA can activate DRG TRPV1 receptors when applied to the intracellular side of the plasma membrane, with greater potency than on the extracellular side (Hwang et al., 2000; Evans et al., 2004). Considering its lower affinity for TRPV1 than CB_1 receptors (Ahluwalia et al., 2003a,b; Ross, 2003), short half-life, and lipophilic nature, AEA is likely to bind to TRPV1 receptors close to its site of synthesis inside the same neuron. This has been demonstrated by the measurement of TRPV1-mediated currents activated from within individual DRG cells by intracellular AEA produced in response to rising $[Ca^{2+}]_i$ (triggered by depletion of intracellular calcium stores) (van der Stelt et al., 2005) or capsaicin (Millns et al., 2006), consistent with the enhancing effects of URB597- on TRPV1-dependent cobalt uptake in this study. Together, these data provide functional evidence for the coexistence of FAAH, AEA, and TRPV1 in DRG neurons.

The proportion of DRG cells positive for Co-ppt after AEA or URB597 treatment was significantly higher when AEA or URB597 were applied with the CB_1 receptor antagonist SR141716. This is consistent with studies demonstrating that antagonism of DRG CB_1 receptors increases the potency of AEA at TRPV1 receptors (Ahluwalia et al., 2003a). At low concentrations, exogenous AEA can reduce TRPV1-evoked excitatory responses via the activation of CB_1 receptors coupled to inhibitory signaling systems (Richardson et al., 1998; Ellington et al., 2002; Ahluwalia et al., 2003b; Evans et al., 2004).

Given the neurochemical phenotype of FAAH-IR neurons, coexpression of CB_1 receptors is unlikely. This is because, under normal uninflamed conditions (with low peripheral NGF levels), the expression of CB_1 receptors on sensory neurons from DRG or trigeminal ganglia is predominantly on large-sized NF200-positive cells (Hohmann and Herkenham, 1999; Bridges et al., 2003; Price et al., 2003; Amaya et al., 2006). Consequently, extracellular AEA produced from FAAH-IR DRG neurons might be expected to signal at CB_1 receptors on separate cells. FAAH also hydrolyzes palmitoylethanolamine (PEA), another endogenous lipid implicated in the modulation of pain responses (Calignano et al., 1998; Jaggar et al., 1998; LoVerme et al., 2005) and a putative ligand for the peroxisome proliferator-activated receptor-α, located on mouse DRG neurons (LoVerme et al., 2006). PEA could compete with AEA for hydrolysis by FAAH and produce entourage effects at TRPV1 receptors (Smart et al., 2002).

FAAH immunoreactivity was detected in the soma of dorsal and ventral horn neurons and those in the dorsal lateral funiculus of spinal cord tissue, matching previous observations (Tsou et al., 1998; Romero et al., 2002). The intracellular location in neuronal soma and dendritic-like processes is consistent with staining observed in brain (Egertová et al., 2003), confirmed at the ultrastructural level (Gulyas et al., 2004). FAAH labeling of white matter areas is consistent with detection of FAAH mRNA (Thomas et al., 1997) and FAAH-IR cells with oligodendrocyte-type morphology in mouse brain (Egertová et al., 2003). Moreover, the colabeling of nucleated FAAH-IR cells with S100 antibodies in sciatic nerve tissue in this study provides evidence that FAAH is expressed in the oligodendrocyte/Schwann cell population labeled by S100 (Palacios et al., 2004).

Axotomy of the sciatic nerve trunk or a spinal nerve branch both produced an increase in the size of ipsilateral FAAH-IR DRG neurons. This, together with costaining with NF200, suggests the induction of FAAH expression in large-sized DRG neurons in response to axonal injury. The neurochemical phenotypes of sensory neuron DRG soma undergo profound changes in response to transection of their peripheral axons. Larger-sized neurons can adopt the phenotypic characteristics of smaller cells (Hudson et al., 2001), such as *de novo* expression of neuropeptides (Hökfelt et al., 1994; Noguchi et al., 1995). These changes are more pronounced when the injury is made closer to the cell body by transecting the spinal nerve (Shortland et al., 1997). Sciatic nerve axotomy reduced TRPV1 labeling in the DRG, as reported previously (Michael and Priestley, 1999) (although this reduction was greater after spinal nerve transection), but the pro-

portion of FAAH-labeled cells was not significantly increased ipsilateral to an axotomy but only after spinal nerve injury. Changes to the size and number of FAAH-IR neurons were more pronounced after injury to the L5 spinal nerve of the sciatic nerve than after peripheral axotomy. SNT injury also produced hypersensivity to cold and mechanical stimuli applied to the ipsilateral hindpaws receiving sciatic nerve innervation. These behavioral changes are synonymous with neuropathic pain behavior in rats (Kim and Chung, 1992; Bridges et al., 2001). *De novo* expression of FAAH on larger NF200-IR neurons after nerve injury may increase colocalization with CB_1 receptor-expressing DRG neurons (Bridges et al., 2003). Although evidence indicates that overall CB_1 receptor expression in the DRG is downregulated after nerve injury (Costigan et al., 2002; Zhang et al., 2007), it is possible that, after axotomy, FAAH activity in larger neurons directly regulates AEA signaling at CB_1 receptors on the same DRG cell. Signaling of AEA may predominate at CB_1 receptors in these conditions, attributable to the downregulation of TRPV1 receptors after injury.

ATF3 labeling in DRG neurons occurs after both types of sciatic nerve injury and is an indicator of neurons in a stress state caused by axonal damage (Tsujino et al., 2000). Increased cellular AEA production is similarly associated with cell damage and concurrent elevations in intracellular calcium, such as those occurring as a result of an excitotoxic or demyelination injury (Baker et al., 2003; Pryce et al., 2003). The presence of ATF3 in most DRG neurons containing FAAH after nerve injury makes it is plausible that the increase in FAAH protein occurs in response to elevated concentrations of AEA induced by axonal damage to the these cells.

A 2 d CFA-induced inflammation of the hindpaw produced behavioral hypersensitivity to mechanical stimuli in common with SNT animals but did not change the size distribution or the number FAAH-IR DRG neurons. This difference could be related to the differential modulation of TRPV1 and CB_1 receptor expression after paw inflammation. In contrast to axotomy injury, CFA-induced inflammation induces *de novo* expression of CB_1 in small neurons, including 67% of the TPRV1-labeled population (Amaya et al., 2006). The number and responsiveness of small TRPV1- and IB4-labeled DRG neurons also increases 2 d after CFA inflammation (Breese et al., 2005). NGF levels (elevated in inflamed tissues) are correlated with the degree of CB_1 and TRPV1 colocalization in cultured DRG neurons (Ahluwalia et al., 2002). AEA overproduction in inflammatory conditions, such as bladder cystitis, has been suggested to mediate prohyperalgesic effects via TRPV1 receptors, in a manner that is potentiated by FAAH inhibitors (Dinis et al., 2004). Whether AEA has a net excitatory or inhibitory effect on DRG neurons can be influenced by several factors, the nature of which affects whether AEA signals predominantly at TRPV1 or CB_1 receptors (Ahluwalia et al., 2003a; Ross, 2003). Consequently, it is plausible that FAAH expression would be differentially regulated in response to specific injury-related changes to its target receptors to control AEA signaling appropriately.

In this study, both anatomical and functional evidence was used to localize the FAAH enzyme, implicated in controlling cellular AEA concentrations, to the soma of peripheral sensory neurons. Its distribution within the neuronal subset with nociceptive functions is modulated by nerve injury. This may be indicative of a role for the endocannabinoid and endovanilloid signaling properties of AEA in modulating peripheral nociceptive transmission.

References

Ahluwalia J, Urban L, Bevan S, Capogna M, Nagy I (2002) Cannabinoid 1 receptors are expressed by nerve growth factor- and glial cell-derived neurotrophic factor-responsive primary sensory neurones. Neuroscience 110:747–753.

Ahluwalia J, Yaqoob M, Urban L, Bevan S, Nagy I (2003a) Activation of capsaicin-sensitive primary sensory neurones induces anandamide production and release. J Neurochem 84:585–591.

Ahluwalia J, Urban L, Bevan S, Nagy I (2003b) Anandamide regulates neuropeptide release from capsaicin-sensitive primary sensory neurones by activating both the cannabinoid 1 receptor and the vannilloid receptor 1 in vitro. Eur J Neurosci 17:2611–2618.

Akiba Y, Kato S, Katsube K, Nakamura M, Takeuchi K, Ishii H, Hibi T (2004) Transient receptor potential vanilloid subfamily 1 expressed in pancreatic islet beta cells modulates insulin secretion in rats. Biochem Biophys Res Commun 321:219–225.

Amaya F, Shimosato G, Kawasaki Y, Hashimoto S, Tanaka Y, Ji RR, Tanaka M (2006) Induction of CB1 cannabinoid receptor by inflammation in primary afferent neurons facilitates antihyperalgesic effect of peripheral CB1 agonist. Pain 124:175–183.

Baker D, Pryce G, Croxford JL, Brown P, Pertwee RG, Makriyannis A, Khanolkar A, Layward L, Fezza F, Bisogno T, Di Marzo V (2001) Endocannabinoids control spasticity in a multiple sclerosis model. FASEB J 15:300–302.

Baker D, Pryce G, Giovannoni G, Thompson AJ (2003) The therapeutic potential of cannabis. Lancet Neurol 2:291–298.

Breese NM, George AC, Pauers LE, Stucky CL (2005) Peripheral inflammation selectively increases TRPV1 function in IB4-positive sensory neurons from adult mouse. Pain 115:37–49.

Bridges D, Ahmad K, Rice AS (2001) The synthetic cannabinoid WIN55,212-2 attenuates hyperalgesia and allodynia in a rat model of neuropathic pain. Br J Pharmacol 133:586–594.

Bridges D, Rice AS, Egertová M, Elphick MR, Winter J, Michael GJ (2003) Localisation of cannabinoid receptor 1 in rat dorsal root ganglion using in situ hybridisation and immunohistochemistry. Neuroscience 119:803–812.

Calignano A, La Rana G, Giuffrida A, Piomelli D (1998) Control of pain initiation by endogenous cannabinoids. Nature 394:277–281.

Calzà L, Pozza M, Zanni M, Manzini CU, Manzini E, Hökfelt T (1998) Peptide plasticity in primary sensory neurons and spinal cord during adjuvant-induced arthritis in the rat: an immunocytochemical and in situ hybridization study. Neuroscience 82:575–589.

Carlton SM, Lekan HA, Kim SH, Chung JM (1994) Behavioral manifestations of an experimental model for peripheral neuropathy produced by spinal nerve ligation in the primate. Pain 56:155–166.

Caterina MJ, Schumacher MA, Tominaga M, Rosen TA, Levine JD, Julius D (1997) The capsaicin receptor: a heat-activated ion channel in the pain pathway. Nature 389:816–824.

Caterina MJ, Leffler A, Malmberg AB, Martin WJ, Trafton J, Petersen-Zeitz KR, Koltzenburg M, Basbaum AI, Julius D (2000) Impaired nociception and pain sensation in mice lacking the capsaicin receptor. Science 288:306–313.

Chang L, Luo L, Palmer JA, Sutton S, Wilson SJ, Barbier AJ, Breitenbucher JG, Chaplan SR, Webb M (2006) Inhibition of fatty acid amide hydrolase produces analgesia by multiple mechanisms. Br J Pharmacol 148:102–113.

Costigan M, Befort K, Karchewski L, Griffin RS, D'Urso D, Allchorne A, Sitarski J, Mannion JW, Pratt RE, Woolf CJ (2002) Replicate high-density rat genome oligonucleotide microarrays reveal hundreds of regulated genes in the dorsal root ganglion after peripheral nerve injury. BMC Neurosci 3:16.

Cravatt BF, Giang DK, Mayfield SP, Boger DL, Lerner RA, Gilula NB (1996) Molecular characterization of an enzyme that degrades neuromodulatory fatty-acid amides. Nature 384:83–87.

Cravatt BF, Demarest K, Patricelli MP, Bracey MH, Giang DK, Martin BR, Lichtman AH (2001) Supersensitivity to anandamide and enhanced endogenous cannabinoid signaling in mice lacking fatty acid amide hydrolase. Proc Natl Acad Sci U S A 98:9371–9376.

Cravatt BF, Saghatelian A, Hawkins EG, Clement AB, Bracey MH, Lichtman AH (2004) Functional disassociation of the central and peripheral fatty acid amide signaling systems. Proc Natl Acad Sci U S A 101:10821–10826.

Cristino L, Starowicz K, De Petrocellis L, Morishita J, Ueda N, Guglielmotti V,

Di Marzo V (2008) Immunohistochemical localization of anabolic and catabolic enzymes for anandamide and other putative endovanilloids in the hippocampus and cerebellar cortex of the mouse brain. Neuroscience 151:955–968.

Deutsch DG, Chin SA (1993) Enzymatic synthesis and degradation of anandamide, a cannabinoid receptor agonist. Biochem Pharmacol 46:791–796.

Deutsch DG, Ueda N, Yamamoto S (2002) The fatty acid amide hydrolase (FAAH). The fatty acid amide hydrolase (FAAH). Prostaglandins Leukot Essent Fatty Acids 66:201–210.

Di Marzo V, Fontana A, Cadas H, Schinelli S, Cimino G, Schwartz JC, Piomelli D (1994) Formation and inactivation of endogenous cannabinoid anandamide in central neurons. Nature 372:686–691.

Dinis P, Charrua A, Avelino A, Yaqoob M, Bevan S, Nagy I, Cruz F (2004) Anandamide-evoked activation of vanilloid receptor 1 contributes to the development of bladder hyperreflexia and nociceptive transmission to spinal dorsal horn neurons in cystitis. J Neurosci 24:11253–11263.

Egertová M, Elphick MR (2000) Localisation of cannabinoid receptors in the rat brain using antibodies to the intracellular C-terminal tail of CB1. J Comp Neurol 422:159–171.

Egertová M, Giang DK, Cravatt BF, Elphick MR (1998) A new perspective on cannabinoid signalling: complementary localization of fatty acid amide hydrolase and CB1 receptor in rat brain. Proc Biol Sci 265:2081–2085.

Egertová M, Cravatt BF, Elphick MR (2003) Comparative analysis of fatty acid amide hydrolase and CB(1) cannabinoid receptor expression in the mouse brain: evidence of a widespread role for fatty acid amide hydrolase in regulation of endocannabinoid signaling. Neuroscience 119:481–496.

Ellington HC, Cotter MA, Cameron NE, Ross RA (2002) The effect of cannabinoids on capsaicin-evoked calcitonin gene-related peptide (CGRP) release from the isolated paw skin of diabetic and non-diabetic rats. Neuropharmacology 42:966–975.

Evans RM, Scott RH, Ross RA (2004) Multiple actions of anandamide on neonatal rat cultured sensory neurones. Br J Pharmacol 141:1223–1233.

Farquhar-Smith WP, Egertová M, Bradbury EJ, McMahon SB, Rice AS, Elphick MR (2000) Cannabinoid CB1 receptor expression in rat spinal cord. Mol Cell Neurosci 15:510–521.

Fegley D, Gaetani S, Duranti A, Tontini A, Mor M, Tarzia G, Piomelli D (2005) Characterization of the fatty acid amide hydrolase inhibitor cyclohexly carbamic acid 3′-carbamoyl-biphenyl-3-yl ester (URB597): effects on anandamide and oleoylethanolamide deactivation. J Pharmacol Exp Ther 313:352–358.

Goldstein ME, House SB, Gainer H (1991) NF-L and peripherin immunoreactivities define distinct classes of rat sensory ganglion cells. J Neurosci Res 30:92–104.

Guindon J, Beaulieu P (2006) Antihyperalgesic effects of local injections of anandamide, ibuprofen, rofecoxib and their combinations in a model of neuropathic pain. Neuropharmacology 50:814–823.

Gulyas AI, Cravatt BF, Bracey MH, Dinh TP, Piomelli D, Boscia F, Freund TF (2004) Segregation of two endocannabinoid-hydrolysing enzymes into pre- and postsynaptic compartments in the rat hippocampus, cerebellum and amygdala. Eur J Neurosci 20:441–458.

Hargreaves K, Dubner R, Brown F, Flores C, Joris J (1988) A new and sensitive method for measuring thermal nociception in cutaneous hyperalgesia. Pain 32:77–88.

Hohmann AG, Herkenham M (1999) Localization of central cannabinoid CB1 receptor messenger RNA in neuronal subpopulations of rat dorsal root ganglia: a double-label in situ hybridization study. Neuroscience 90:923–931.

Hohmann AG, Suplita RL, Bolton NM, Neely MH, Fegley D, Mangieri R, Krey JF, Walker JM, Holmes PV, Crystal JD, Duranti A, Tontini M, Mor M, Tarzia G, Piomelli D (2005) An endocannabinoid mechanism for stress-induced analgesia. Nature 435:1108–1112.

Hökfelt T, Zhang X, Wiesenfeld-Hallin Z (1994) Messenger plasticity in primary sensory neurons following axotomy and its functional implications. Trends Neurosci 17:22–30.

Holt S, Comelli F, Costa B, Fowler CJ (2005) Inhibitors of fatty acid amide hyrdolase reduce carrageenan-induce hind paw inflammation in pentobarbital-treated mice: comparison with indomethacin and possible involvement of cannabinoid receptors. Br J Pharmacol 146:467–476.

Hudson LJ, Bevan S, Wotherspoon G, Gentry C, Fox A, Winter J (2001) VR1 protein expression increases in undamaged DRG neurons after partial nerve injury. Eur J Neurosci 13:2105–2114.

Hwang SW, Cho H, Kwak J, Lee SY, Kang CJ, Jung J, Cho S, Min KH, Suh YG, Kim D, Oh U (2000) Direct activation of capsaicin receptors by products of lipoxygenase: endogenous capsaicin-like substances. Proc Natl Acad Sci U S A 97:6155–6160.

Jaggar SI, Hasnie FS, Sellaturay S, Rice ASC (1998) The anti-hyperalgesic actions of the cannabinoid anandamide and the putative CB2 agonist palmitoylethanolamide in models of visceral and somatic inflammatory pain. Pain 76:189–199.

Jayamanne A, Greenwood R, Mitchell VA, Aslan S, Piomelli D, Vaughan CW (2006) Actions of the FAAH inhibitor URB597 in neuropathic and chronic inflammatory pain models. Br J Pharmacol 147:281–288.

Jhaveri MD, Richardson D, Kendall DA, Barrett DA, Chapman V (2006) Analgesic effects of fatty acid amide hydrolase inhibition in a rat model of neuropathic pain. J Neurosci 26:13318–13327.

Ji RR, Samad TA, Jin SX, Schmoll R, Woolf CJ (2002) p38 MAPK activation by NGF in primary sensory neurons after inflammation increases TRPV1 levels and maintains heat hyperalgesia. Neuron 36:57–68.

Kim SH, Chung JM (1992) An experimental model for peripheral neuropathy produced by segmental spinal nerve ligation in the rat. Pain 50:355–363.

Kozak KR, Marnett LJ (2002) Oxidative metabolism of endocannabinoids. Prostaglandins Leukot Essent Fatty Acids 66:211–220.

Lawson SN, Waddell PJ (1991) Soma neurofilament immunoreactivity is related to cell size and fibre conduction velocity in rat primary sensory neurons. J Physiol 435:41–63.

Ledent C, Valverde O, Cossu G, Petitet F, Aubert JF, Beslot F, Böhme GA, Imperato A, Pedrazzini T, Roques BP, Vassart G, Fratta W, Parmentier M (1999) Unresponsiveness to cannabinoids and reduced addictive effects of opiates in CB1 receptor knockout mice. Science 283:401–404.

Lichtman AH, Shelton CC, Advani T, Cravatt BF (2004a) Mice lacking fatty acid amide hydrolase exhibit a cannabinoid receptor-mediated phenotypic hypoalgesia. Pain 109:319–327.

Lichtman AH, Leung D, Shelton CC, Saghatelian A, Hardouin C, Boger DL, Cravatt BF (2004b) Reversible inhibitors of fatty acid amide hydrolase that promote analgesia: evidence for an unprecedented combination of potency and selectivity. J Pharmacol Exp Ther 311:441–448.

Liu M, Willmott NJ, Michael GJ, Priestley JV (2004) Differential pH and capsaicin responses of *Griffonia simplicifolia* IB4 (IB4)-positive and IB4-negative small sensory neurons. Neuroscience 127:659–672.

LoVerme J, La Rana G, Russo R, Calignano A, Piomelli D (2005) The search for the palmitoylethanolamide receptor. Life Sci 77:1685–1698.

LoVerme J, Russo R, La Rana G, Fu J, Farthing J, Mattace-Raso G, Meli R, Hohmann A, Calignano A, Piomelli D (2006) Rapid broad-spectrum analgesia through activation of peroxisome proliferator-activated receptor-alpha. J Pharmacol Exp Ther 319:1051–1061.

Michael GJ, Priestley JV (1999) Differential expression of the mRNA for the vanilloid receptor subtype 1 in cells of the adult rat dorsal root and nodose ganglia and its downregulation by axotomy. J Neurosci 19:1844–1854.

Michael GJ, Averill S, Nitkunan A, Rattray M, Bennett DL, Yan Q, Priestley JV (1997) Nerve growth factor treatment increases brain-derived neurotrophic factor selectively in TrkA-expressing dorsal root ganglion cells and in their central terminations within the spinal cord. J Neurosci 17:8476–8490.

Millns PJ, Chimenti M, Ali N, Ryland E, de Lago E, Fernandez-Ruiz J, Chapman V, Kendall DA (2006) Effects of inhibition of fatty acid amide hydrolase vs the anandamide membrane transporter on TRPV1-mediated calcium responses in adult DRG neurons; the role of CB receptors. Eur J Neurosci 24:3489–3495.

Möller KA, Johansson B, Berge OG (1998) Assessing mechanical allodynia in the rat paw with a new electronic algometer. J Neurosci Methods 84:41–47.

Mor M, Rivara S, Lodola A, Plazzi PV, Tarzia G, Duranti A, Tontini A, Piersanti G, Kathuria S, Piomelli D (2004) Cyclohexylcarbamic acid 3′- or 4′ substituted biphenyl-3-yl esters as fatty acid amide hydrolase inhibitors: synthesis, quantitative structure-activity relationships and molecular modeling studies. J Med Chem 47:4998–5008.

Muthian S, Rademacher DJ, Roelke CT, Gross GJ, Hillard CJ (2004) Anandamide content is increased and CB1 cannabinoid receptor blockade is protective during transient, focal cerebral ischemia. Neuroscience 129:743–750.

Nagy I, Pabla R, Matesz C, Dray A, Woolf CJ, Urban L (1993) Cobalt uptake enables identification of capsaicin- and bradykinin-sensitive subpopulations of rat dorsal root ganglion cells in vitro. Neuroscience 56:241–246.

Noguchi K, Kawai Y, Fukuoka T, Senba E, Miki K (1995) Substance P induced by peripheral nerve injury in primary afferent sensory neurons and its effect on dorsal column nucleus neurons. J Neurosci 15:7633–7643.

Ortega-Gutiérrez S, Hawkins EG, Viso A, López-Rodríguez ML, Cravatt BF (2004) Comparison of anandamide transport in FAAH wild-type and knockout neurons: evidence for contributions by both FAAH and the CB1 receptor to anandamide uptake. Biochemistry 43:8184–8190.

Palacios G, Muro A, Verdú E, Pumarola M, Vela JM (2004) Immunohistochemical localization of the sigma1 receptor in Schwann cells of rat sciatic nerve. Brain Res 1007:65–70.

Patricelli MP, Lashuel HA, Giang DK, Kelly JW, Cravatt BF (1998) Comparative characterization of a wild type and transmembrane domain-deleted fatty acid amide hydrolase: identification of the transmembrane domain as a site for oligomerization. Biochemistry 37:15177–15187.

Piomelli D, Beltramo M, Giuffrida A, Stella N (1998) Endogenous cannabinoid signalling. Neurobiol Dis 5:462–473.

Potrebic S, Ahn AH, Skinner K, Fields HL, Basbaum AI (2003) Peptidergic nociceptors of both trigeminal and dorsal root ganglia express serotonin 1D receptors: implications for the selective antimigraine action of triptans. J Neurosci 23:10988–10997.

Price TJ, Helesic G, Parghi D, Hargreaves KM, Flores CM (2003) The neuronal distribution of cannabinoid receptor type 1 in the trigeminal ganglion of the rat. Neuroscience 120:155–162.

Price TJ, Patwardhan AM, Flores CM, Hargreaves KM (2005) A role for the anandamide membrane transporter in TRPV1-mediated neurosecretion from trigeminal sensory neurons. Neuropharmacology 49:25–39.

Pryce G, Ahmed Z, Hankey DJ, Jackson SJ, Croxford JL, Pocock JM, Ledent C, Petzold A, Thompson AJ, Giovannoni G, Cuzner ML, Baker D (2003) Cannabinoids inhibit neurodegeneration in models of multiple sclerosis. Brain 126:2191–2202.

Richardson JD, Kilo S, Hargreaves KM (1998) Cannabinoids reduce hyperalgesia and inflammation via interaction with peripheral CB1 receptors. Pain 75:111–119.

Romero J, Hillard CJ, Calero M, Rábano A (2002) Fatty acid amide hydrolase localisation in the human central nervous system: an immunohistochemical study. Mol Brain Res 100:85–93.

Ross RA (2003) Anandamide and vanilloid TRPV1 receptors. Br J Pharmacol 140:790–801.

Ross RA, Coutts AA, McFarlane SM, Anavi-Goffer S, Irving AJ, Pertwee RG, MacEwan DJ, Scott RH (2001) Actions of cannabinoid receptor ligands on rat cultured sensory neurones: implications for antinociception. Neuropharmacology 40:221–232.

Russo R, Loverme J, La Rana G, Compton TR, Parrott J, Duranti A, Tontini A, Mor M, Tarzia G, Calignano A, Piomelli D (2007) The fatty acid amide hydrolase inhibitor URB597 (cyclohexylcarbamic acid 3′-carbamoylbiphenyl-3-yl ester) reduces neuropathic pain after oral administration in mice. J Pharmacol Exp Ther 322:236–242.

Sathianathan V, Avelino A, Charrua A, Santha P, Matesz K, Cruz F, Nagy I (2003) Insulin induces cobalt uptake in a subpopulation of rat cultured primary sensory neurones. Eur J Neurosci 18:2477–2486.

Shortland P, Kinman E, Molander C (1997) Sprouting of A-fibre primary afferents into lamina II in two rat models of neuropathic pain. Eur J Pain 1:215–227.

Singh Tahim A, Sántha P, Nagy I (2005) Inflammatory mediators convert anandamide into a potent activator of the vanilloid type 1 transient receptor potential receptor in nociceptive primary sensory neurons. Neuroscience 136:539–548.

Smart D, Jonsson KO, Vandevoorde S, Lambert DM, Fowler CJ (2002) "Entourage" effects of N-acyl ethanolamines at human vanilloid receptors. Comparison of effects upon anandamide-induced vanilloid receptor activation and upon anandamide metabolism. Br J Pharmacol 136:452–458.

Snider WD, McMahon SB (1998) Tackling pain at the source: new ideas about nociceptors. Neuron 20:629–632.

Thomas EA, Cravatt BF, Danielson PE, Gilula NB, Sutcliffe JG (1997) Fatty acid amide hydrolase, the degradative enzyme for anandamide and oleamide, has selective distribution in neurons within the rat central nervous system. J Neurosci Res 50:1047–1052.

Tsou K, Nogueron MI, Muthian S, Sañudo-Pena MC, Hillard CJ, Deutsch DG, Walker JM (1998) Fatty acid amide hydrolase is located preferentially in large neurons in the rat central nervous system as revealed by immunohistochemisty. Neurosci Lett 254:137–140.

Tsujino H, Kondo E, Fukuoka T, Dai Y, Tokunaga A, Miki K, Yonenobu K, Ochi T, Noguchi K (2000) Activating transcription factor 3 (ATF3) induction by axotomy in sensory and motorneurones: a novel neuronal marker of nerve injury. Mol Cell Neurosci 15:170–182.

van der Stelt M, Trevisani M, Vellani V, De Petrocellis L, Schiano Moriello A, Campi B, McNaughton P, Geppetti P, Di Marzo V (2005) Anandamide acts as an intracellular messenger amplifying Ca^{2+} influx via TRPV1 channels. EMBO J 24:3026–3037.

Walker JM, Huang SM, Strangman NM, Tsou K, Sañudo-Peña MC (1999) Pain modulation by release of the endogenous cannabinoid anandamide. Proc Natl Acad Sci U S A 96:12198–12203.

Zhang F, Hong S, Stone V, Smith PJ (2007) Expression of cannabinoid CB_1 receptors in models of diabetic neuropathy. J Pharmacol Exp Ther 323:508–515.

Zygmunt PM, Petersson J, Andersson DA, Chuang H, Sørgård M, Di Marzo V, Julius D, Högestätt ED (1999) Vanilloid receptors on sensory nerves mediate the vasodilator action of anandamide. Nature 400:452–457.